Earth and Planetary Science Letters 568 (2021) 117034

Contents lists available at ScienceDirect

Earth and Planetary Science Letters

www.elsevier.com/locate/epsl

Mantle sources and magma evolution in Europe's largest rare earth element belt (Gardar Province, SW Greenland): New insights from sulfur isotopes

William Hutchison [a,*], Adrian A. Finch [a], Anouk M. Borst [a], Michael A.W. Marks [b], Brian G.J. Upton [c], Aubrey L. Zerkle [a], Eva E. Stüeken [a], Adrian J. Boyce [d]

[a] School of Earth and Environmental Sciences, University of St Andrews, KY16 9AL, UK
[b] Mathematisch-Naturwissenschaftliche Fakultät, FB Geowissenschaften, Universität Tübingen, Wilhelmstrasse 56, 72074 Tübingen, Germany
[c] School of GeoSciences, University of Edinburgh, Edinburgh EH9 3JW, UK
[d] Scottish Universities Environmental Research Centre, Rankine Avenue, East Kilbride G75 0QF, UK

ARTICLE INFO

Article history:
Received 29 October 2020
Received in revised form 6 May 2021
Accepted 29 May 2021
Available online xxxx
Editor: R. Hickey-Vargas

Keywords:
rift
magmatism
sulfur
geochemistry
REE
volatiles

ABSTRACT

Alkaline igneous complexes are often rich in rare earth elements (REE) and other metals essential for modern technologies. Although a variety of magmatic and hydrothermal processes explain the occurrence of individual deposits, one common feature identified in almost all studies, is a REE-enriched parental melt sourced from the lithospheric mantle. Fundamental questions remain about the origin and importance of the mantle source in the genesis of REE-rich magmas. In particular, it is often unclear whether localized enrichments within an alkaline province reflect heterogeneity in the mantle source lithology (caused by prior subduction or plume activity) or variations in the degree of partial melting and differentiation of a largely homogeneous source. Sulfur isotopes offer a means of testing these hypotheses because they are unaffected by high temperature partial melting processes and can fingerprint different mantle sources. Although one must be careful to rule out subsequent isotope fractionation during magma ascent, degassing and crustal interactions.

Here, we present new S concentration and isotope ($\delta^{34}S$) measurements, as well as a compilation of major and trace element data, for a suite of alkaline magmatic units and crustal lithologies from the Mesoproterozoic Gardar Province. Samples span all phases of Gardar magmatism (1330–1140 Ma) and include regional dykes, rift lavas and the alkaline complexes Motzfeldt and Ilímaussaq, which represent two of Europe's largest REE deposits. We show that the vast majority of our 115 samples have S contents $>$100 ppm and $\delta^{34}S$ of -1 to 5‰. Only 8 samples (with low S contents, $<$100 ppm) show evidence for crustal interactions, implying that the vast majority of Gardar melts preserve the S isotopic signature of their magma source. Importantly, samples from across the Gardar Province have $\delta^{34}S$ above the canonical mantle range (≤ -1.4‰) and therefore require recycled surface S in their mantle source. Elevated $\delta^{34}S$ values are explained by a period of Andean-style subduction and mantle metasomatism which took place $\sim$500 Ma before rift onset and are also supported by trace elements signatures (e.g. Ba/La) which match modern subduction zones.

Comparing the various generations of Gardar magmas, we find that $\delta^{34}S$ values, large ion lithophile elements (K, Ba, P) and selective incompatible elements (Nb and light REE) are particularly enriched in the Late Gardar dykes, alkaline complexes and clusters of silica-undersaturated dykes spatially associated with the alkaline complexes. These data indicate that subduction-related metasomatism of the Gardar mantle was spatially heterogeneous, and that alkaline complexes are sourced from localized mantle domains highly enriched in ^{34}S, REE, alkalis and volatiles (particularly, F). Since alkalis and volatiles play an essential role in driving extreme differentiation of alkaline melts and fluids, we suggest the co-location of these species plus incompatible metals at high concentrations in the lithospheric mantle is a critical first-step in the genesis of a world-class alkaline REE deposit. S isotopes are powerful tools for identifying enriched mantle domains and the sources of mineralized alkaline igneous bodies.

* Corresponding author.
E-mail address: wh39@st-andrews.ac.uk (W. Hutchison).

https://doi.org/10.1016/j.epsl.2021.117034

1. Introduction

Alkaline igneous rocks are important natural sources of rare earth elements (REE) and high field-strength elements (HFSE) (Kogarko, 1990). Although a variety of processes influence the total REE and HFSE content of alkaline systems, numerous studies highlight the importance of an enriched lithospheric mantle in the genesis of the largest ore bodies (Lehmann et al., 1994). The precise role of the mantle source in generating REE- and HFSE-rich melts remains uncertain; there is ongoing debate as to whether source enrichments relate to ancient subduction or mantle plume processes (Hulett et al., 2016), and whether source enrichment is critical for generating world-class alkaline igneous deposits (Smith et al., 2016).

One of the most significant regions of REE and HFSE enrichment in Europe is the Gardar Province, a Mesoproterozoic continental rift located in south-west Greenland (Fig. 1). The Gardar hosts extrusive and intrusive alkaline igneous rocks. The most chemically evolved rocks are associated with km-scale alkaline complexes (Upton, 2013). Notable are Motzfeldt and Ilímaussaq which are among the world's largest alkaline ore deposits (Marks and Markl, 2015; Finch et al., 2019). Although Motzfeldt and Ilímaussaq show many geochemical affinities (Schönenberger and Markl, 2008) and are separated by $<$50 km, geochronology reveals that they are separated in time by $\sim$100 Ma (McCreath et al., 2012; Borst et al., 2019). The primitive melts that fed these complexes have been linked to an enriched lithospheric mantle source, but it is unclear how heterogeneous this mantle was and whether enrichment originated from prior subduction (Bartels et al., 2015) or plume processes (Halama et al., 2003). A greater understanding of Gardar mantle sources is critical to elucidating the origins of Motzfeldt and Ilímaussaq (and large alkaline ore deposits generally) because it is unclear whether their REE and HFSE enrichment reflects similar magmatic processes (i.e. degree of partial melting and fractionation) or similar mantle sources.

Sulfur isotopes (δ^{34}S) are excellent tracers of mantle sources because they are not significantly fractionated by high temperature mantle melting processes (Labidi and Cartigny, 2016). Initial δ^{34}S values can, however, be modified during magma ascent as melts degas, crystallize S bearing minerals, and assimilate local crust (Marini et al., 2011). To date, no study has analyzed δ^{34}S across a full spectrum of rift-related alkaline rocks, rigorously assessed magmatic and crustal modifications and identified the magmatic suites that offer the best constraints on mantle δ^{34}S.

The Gardar Province provides a window into the shallow plumbing system of an ancient rift ($\sim$3–4 km depths, Upton, 2013) and is an ideal setting for this study. We present a detailed S isotope investigation of all major magmatic suites intruded and erupted across the province over multiple phases of rifting. By analyzing the δ^{34}S of crustal lithologies and modeling S degassing and sulfide fractionation we identify samples where magmatic processes have modified initial δ^{34}S. We show that primitive mafic dykes record the δ^{34}S of their magma source. Our data emphasize the importance of prior subduction in seeding incompatible, alkali and volatile element enriched mantle domains and suggest these processes are critical to the formation of alkaline ore deposits.

2. Geological setting

Gardar magmas are intruded across the boundary between the North Atlantic Craton ($>$2800 Ma Archean orthogneiss) and the Paleoproterozoic mobile belt ($\sim$1800 Ma Ketilidian granites, Fig. 1, Upton, 2013). Magmatism occurred in two distinct phases between 1330–1260 Ma and 1180–1140 Ma, referred to as Early and Late Gardar, respectively. The Early Gardar is represented by evolved alkaline complexes (e.g. Motzfeldt and Ivigtût), E-W mafic dykes, and a sequence of rift-related sedimentary and volcanic rocks known as the Eriksfjord Formation. Eriksfjord volcanics are mostly sub-aerial lavas and are subdivided into upper, middle and lower units (cf. Halama et al., 2003).

The Late Gardar is represented by alkaline complexes (e.g. Ilímaussaq and Nunarsuit), ENE-WSW mafic dyke swarms and two giant ($\leq$800 m wide) dyke complexes (GDC, mainly comprising gabbroic cumulate but with some syenitic bodies). Late Gardar dykes are only found in the mobile belt and are concentrated in two magmatic segments: the Tuttutooq–Ilimmaasaq–Narsarsuaq (TIN) and Nunarsuit-Isortoq (NI) zones (Fig. 1c). Small volumes of lamprophyres and carbonatites were also erupted at various times throughout the Gardar and represented by clusters of diatremes and intrusive plugs (Coulson et al., 2003).

Gardar alkaline complexes are usually multi-phase (represented by quartz- and nepheline-bearing syenites with subordinate alkali granite and carbonatite), and show extreme enrichment in alkalis, halogens, HFSE and other REE (Marks and Markl, 2015). Alkaline complexes and giant dykes (above) show well-developed cumulate layering and formed via protracted fractional crystallization of alkali basaltic parental melts (Upton, 2013). Geochemical investigations find little evidence for crustal contamination (Marks et al., 2004), although a few analyses of samples from the roof and margins of the complexes support localized anatexis (Stevenson et al., 1997).

It is suggested that Gardar magmas derive from metasomatized lithospheric mantle (Köhler et al., 2009; Bartels et al., 2015) and that metasomatism linked to a period of northward subduction during the Ketilidian (Fig. 1b). However, it is unclear whether metasomatism led to local- or regional-scale enrichment of the mantle, and whether there exist lateral (north-south) gradients in metasomatism (as expected above a subducting slab, e.g. Watt et al., 2013).

3. Material and methods

We examined S concentrations and δ^{34}S in representative whole-rock samples from across the Gardar (115 samples, see Supplementary Information for notes on sample preparation and Supplementary Data 1 for detailed descriptions). Samples include Archean and Ketilidian basement; Eriksfjord country rocks; primitive mafic dykes; gabbroic to syenitic giant dykes, and multi-phase alkaline complexes hosting REE and HFSE deposits. For the alkaline complexes and mafic dykes, we analyzed a few samples adjacent to country rock and country rock xenoliths (within 0.1–10 m) to evaluate potential magma-crust interactions and impacts on δ^{34}S.

S concentrations were determined by Combustion Ion Chromatography at the Universität Tübingen using a 930 Compact IC Flex chromatograph (Metrohm) combined with a combustion oven (Analytik Jena). The effective detection limit was 1–2 µg/g, and repeated analyses of samples and reference material GSN showed relative uncertainties were generally $<$15% (1σ).

For δ^{34}S, we extracted sulfide phases from whole-rock powders as Ag_2S via sequential reflux with 6M HCl and ethanol followed by acidified 1 M $CrCl_2$ (Canfield et al., 1986). We collected Ag_2S precipitates before and after the addition of the $CrCl_2$ solution. The first precipitate is the acid volatile sulfur (AVS); the second precipitate is the chromium reducible sulfur (CRS). CRS typically

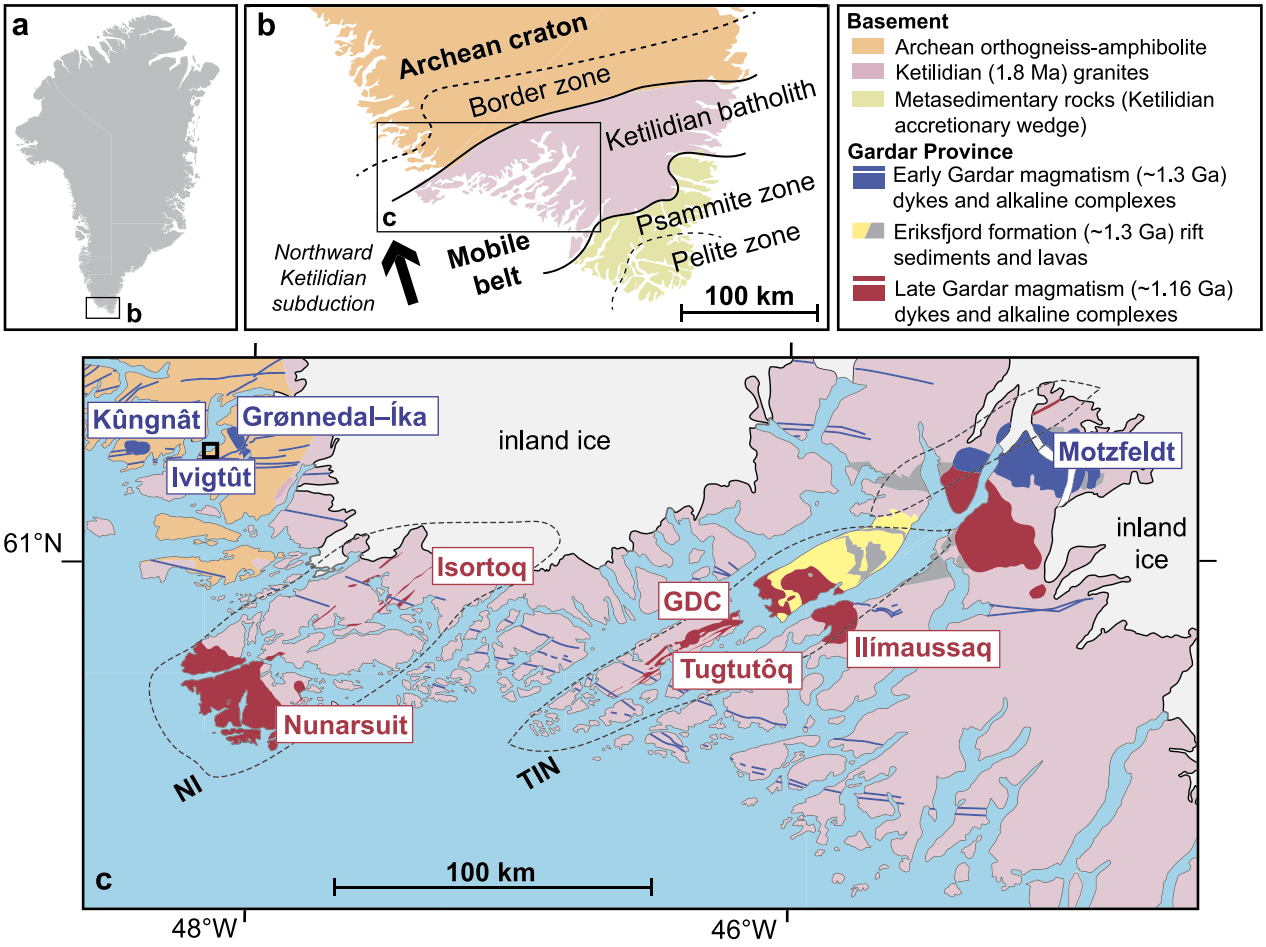

Fig. 1. Geographic and geological setting of the Mesoproterozoic Gardar alkaline province in south Greenland (a). Magmas were emplaced into Archean and Ketilidian basement (b), and the latter formed during a period of Andean-style subduction in the Paleoproterozoic (~1.8 Ga). A regional geological map of south-west Greenland (c) shows the distribution of magmatism in the alkaline province (modified after Sørensen et al., 2006). Blue colors correspond to Early Gardar magmatism while red colors to Late Gardar magmatism (these were centered around ~1.3 Ga and ~1.16 Ga, respectively). The Late Gardar dyke swarms are concentrated in the Nunarsuit–Isortoq (NI) and Tuttutooq–Ilimmaasaq–Narsarsuaq (TIN) magmatic segments and are outlined by the dashed black lines. Note that two giant dyke complexes (GDC) associated with the Tugtutôq complex are classified as Older and Younger but both occur in the Late Gardar. Rift-related lavas and terrestrial sandstones comprising the Eriksfjord Formation are linked to Early Gardar magmatism. Please note that we follow the nomenclature of earlier studies (Upton, 2013), adopting modern Greenlandic spelling for geographical features (i.e. Tuttutooq island and Ilimmaasaq mountain), and pre-1973 spelling for geological features (Tugtutôq and Ilímaussaq intrusive complexes). (For interpretation of the colors in the figure(s), the reader is referred to the web version of this article.)

accounts for 70–100% of the total S yield. While it is commonly assumed that AVS comprises monosulfides (e.g. sphalerite, galena and pyrrhotite) and CRS comprises elemental S and disulfides (e.g. pyrite), it is demonstrated that many sulfides are partially soluble in hot HCl and extracted as both AVS and CRS (Praharaj and Fortin, 2004). Our plots show bulk $\delta^{34}S$, and AVS and CRS $\delta^{34}S$ as these provide insights into $\delta^{34}S$ heterogeneity of the samples. For Ilímaussaq and Motzfeldt, Hutchison et al. (2019) measured $\delta^{34}S$ in sulfide minerals separated from nepheline syenite dykes, sills, and hydrothermal veins. These samples are compared with our bulk-rock $\delta^{34}S$ and it should be noted that they compare rocks of similar composition, rather than identical samples.

S isotope analysis was undertaken at the Scottish Universities Environmental Research Centre (SUERC) and the School of Earth and Environmental Sciences (University of St Andrews). An Isoprime VisION isotope ratio mass spectrometer (IRMS) with a linked Vario PYRO cube elemental analyzer (EA) was used at SUERC and an EA IsoLink, coupled to a MAT 253 IRMS was used at St Andrews. Standard data were within ±0.2‰ of accepted values and replicates between the laboratories were consistent to the error within natural $\delta^{34}S$ heterogeneity (generally, ±0.4‰ at 2σ).

We compiled whole-rock major and trace element data for lavas and dykes across the Gardar. The compilation and processing procedure is fully described in the Supplementary Information. Note that relative errors for major elements are generally <2%, and 5–20% for trace elements (these uncertainties are mostly captured by the data symbols in our plots).

4. Results

4.1. Models of S isotope fractionation caused by assimilation, degassing and fractional crystallization

Various magmatic processes alter the initial $\delta^{34}S$. Magma-crust interaction is a prime example. The three main Gardar crustal lithologies (Eriksfjord sediments, Archean orthogneiss and Ketilidian granites, Fig. 1) are notable for their low S concentrations (6–99 ppm) but variable $\delta^{34}S$ (0–25‰, Supplementary Information). To evaluate magma-crust interactions, we generated a two-component mixing model between each crustal lithology and an uncontaminated (0‰) magmatic end-member with initial S concentrations of 50, 100, 500 and 1000 ppm (full details of this and subsequent isotope modeling are provided in the Supplementary Information). Assimilation of Eriksfjord sediments may lead to significant $\delta^{34}S$ increases (Fig. 2a), but only in samples where magmatic S contents are very low (≤100 ppm). Assimilation of

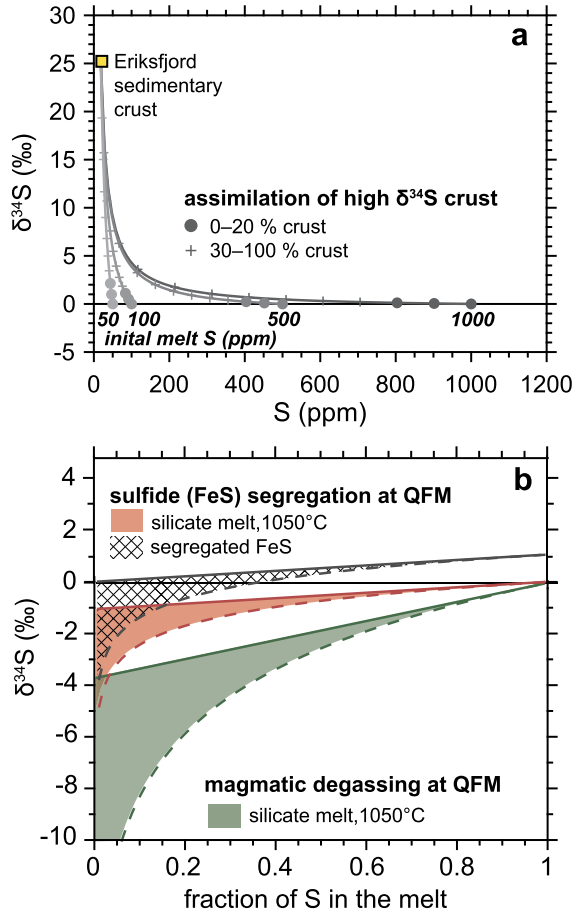

Fig. 2. Summary of magmatic processes that modify δ^{34}S. **a)** Magma-crust interactions are examined using a binary mixing model. A mantle derived melt (with $\delta^{34}S = 0‰$, and variable S concentration) is contaminated by an Eriksfjord sandstone (with $\delta^{34}S = 25‰$ and S = 19 ppm, the average of multiple analyses, Supplementary Data 1). Mixing between these endmembers is shown in increments of 10%. Note that previous isotopic and trace element investigations of crustal interactions indicated low levels of assimilation 0–20% (Stevenson et al., 1997; Marks et al., 2004; Bartels et al., 2015). Hence, distinct symbols are used to distinguish these data points. **b)** The impact of S degassing and sulfide mineral, FeS, fractionation (segregation) on melt δ^{34}S. In both models initial melts have $\delta^{34}S = 0‰$, and a relatively reduced redox buffer is used (fO_2 = QFM, in good agreement with petrological constraints, Upton and Thomas, 1980; Upton et al., 1985; Schönenberger and Markl, 2008; Marks and Markl, 2015). Open and closed-system processes (Marini et al., 1994) are shown by the dashed and solid lines, respectively, and thus the shaded area between these lines gives the range of δ^{34}S values expected (degassing melt: green; melt crystallizing FeS: red; and segregated FeS: hatched). Note that our calculations adopt the equations of Marini et al. (2011), the melt S speciation models of Jugo et al. (2010), and the silicate melt fractionation factors of Fiege et al. (2015), and are fully described in the Supplementary Information.

Archean and Ketilidian crust generates minor increases in δ^{34}S (<0.6‰, Supplementary Figure 2) comparable to the natural δ^{34}S heterogeneity observed in these samples (Section 3).

Sulfur degassing affects the δ^{34}S of S dissolved in silicate melt (Marini et al., 2011). The extent of S degassing is controlled by pressure, while the redox conditions, i.e. the ratio of reduced to oxidized S, govern the magnitude and sign of δ^{34}S fractionation. In Fig. 2b we model degassing of a magma with an oxygen fugacity (fO_2) at the QFM buffer. QFM is a reasonable assumption because all petrological investigations of Gardar magmas have consistently reported fO_2 at or below QFM (Upton and Thomas, 1980; Schönenberger and Markl, 2008). At an fO_2 of QFM, reduced S species prevail in the melt (Jugo et al., 2010; Fiege et al., 2015), H_2S is the main degassing phase (Marini et al., 2011), and our models predict extreme low-δ^{34}S in samples that have experienced extensive S degassing ($\ll -4‰$). An important caveat is that previous investigations of magmatic degassing (e.g. Aiuppa et al., 2007) show greatest S degassing at pressures <25 MPa. Stratigraphic reconstructions and fluid inclusion data for the Gardar suggest our samples are representative of 3–4 km depths, hence pressures of ~100 MPa (Upton et al., 2003; Krumrei et al., 2007). Therefore, it is unlikely that Gardar magmas have undergone extensive degassing.

Sulfide mineral segregation during magma evolution and fractionation also affects the δ^{34}S of silicate melt. A model for a magma at QFM is shown in Fig. 2b. Results show that segregated sulfide (FeS) has slightly higher δ^{34}S than the melt; this causes a decrease in δ^{34}S in the residual melt. Compared to degassing processes, δ^{34}S fractionation by sulfide segregation is much less extreme. For complete closed-system fractionation, δ^{34}S changes by $\leq 1‰$. For open-system fractionation, the melt needs to lose 60% of its total S before δ^{34}S changes by more than 1‰. Thus, sulfide segregation leads to large changes in S concentration but limited measurable variation in δ^{34}S (since sample heterogeneity is $\pm 0.4‰$).

4.2. Sulfur isotopes and concentrations

Fig. 3 shows whole-rock δ^{34}S and S concentrations for the Older and Younger giant dyke complexes (OGDC and YGDC) which both formed in Late Gardar times. OGDC gabbros have a narrow range of S concentrations (700–820 ppm) and bulk δ^{34}S between −0.1 and 1.3‰ (Fig. 3a). Basanitic melt from the chilled margin of the OGDC shows comparable δ^{34}S and slightly higher S content, while syenitic cumulate shows the lowest S concentration and bulk δ^{34}S. Gabbros from the YGDC border facies show low S concentrations (50–130 ppm), while those from the central facies have S concentrations of ~500 ppm. Interestingly, Upton and Thomas (1980) reported much higher S concentrations (~2000 ppm, Fig. 3b) in different YGDC gabbro samples and a basalt from the chilled margin. YGDC syenites exhibit similar δ^{34}S to the gabbros we analyzed but higher S contents of 1000–1400 ppm.

Fig. 4 shows results for alkaline complexes. At Ilímaussaq, most whole-rock samples with S contents >100 ppm show δ^{34}S of 1–2‰. Fig. 4b shows δ^{34}S of sulfide minerals separated from reduced hydrothermal veins and late-stage nepheline syenite dykes and sills (lujavrites) by Hutchison et al. (2019). Sulfide separates show a wide range of δ^{34}S, although sphalerites show good overlap with whole-rock δ^{34}S from the various magmatic units. This reflects the fact that sphalerite is often the main S-bearing phase in Ilímaussaq syenites (Supplementary Data 1), and that sphalerite-melt fractionation is minimal at magmatic temperatures ($\leq 0.3‰$ between 1000–300 °C, Ohmoto and Rye, 1979). To evaluate crustal interactions, we analyzed peralkaline granites in the roof of Ilímaussaq, and lujavrites from its margins (10–100 m, from in situ Eriksfjord country rocks). Peralkaline granites exhibit low S contents (15–30 ppm) and remarkably high-δ^{34}S (21.5‰). The lujavrites in this study were sampled adjacent to Eriksfjord country rock xenoliths; their whole-rock δ^{34}S (3–6‰) is slightly greater than the δ^{34}S of sphalerite separates from xenolith-free lujavrites (analyzed previously by Hutchison et al., 2019).

Motzfeldt is represented by nested syenitic bodies and whole-rock S concentrations are 10–215 ppm (Fig. 4c). Unaltered syenites from the Flinks Dal, North Qôroq and North Motzfeldt centers show δ^{34}S of 0–2‰. Motzfeldt Sø syenites, which host a large HFSE deposit of major economic interest, show a wider δ^{34}S range (−5 to 12‰). Motzfeldt Sø syenites are distinct from the other magmatic centers because: 1) they are in direct contact with Eriksfjord country rock in the roof of the complex, and 2) they are hydrothermally altered and cross-cut by irregular late-stage veins (Finch et al., 2019). Motzfeldt Sø syenites with high-δ^{34}S (up to 12‰,

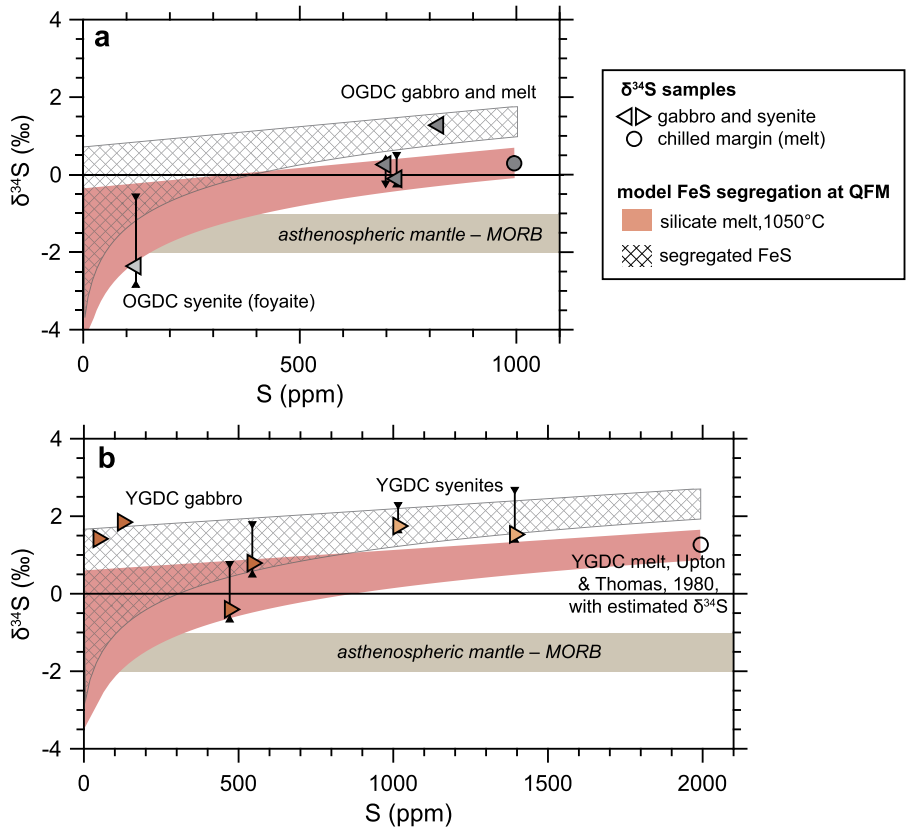

Fig. 3. S concentration and δ^{34}S for the Older and Younger giant dyke complex (OGDC and YGDC, in **a** and **b**, respectively). Most samples are either gabbroic or syenitic cumulate (shown as triangles) although one sample from the chilled margin of the OGDC is also included (shown as the colored a circle). For each sample bulk δ^{34}S is shown by the large colored symbol. For samples with distinguishable acid volatile sulfur (AVS) a black vertical line connects the δ^{34}S of their AVS (downward pointing triangle) and chromium reducible sulfur (CRS, upward pointing triangle). Models of sulfide mineral (FeS) fractionation (Section 4.1) are overlain on each plot. The red shaded area shows the silicate melt evolution, while the hatched area shows the segregated FeS evolution. Note that the upper and lower limits of each area are given by the equations for open and closed-system processes, respectively (after Marini et al., 1994). For the OGDC, we use the sample from the chilled margin of the dyke as a parental composition. For the YGDC, we did not make new S concentration and δ^{34}S analyses for a chilled margin sample and instead used a S concentration measurement from Upton and Thomas (1980) and averaged the δ^{34}S of contemporaneous Late Gardar dykes on the Tuttutooq archipelago adjacent to the YGDC. The beige horizontal bar indicates the δ^{34}S of the asthenospheric mantle as sampled by MORB (Labidi et al., 2013).

Fig. 4c) are from microsyenite dykes in the uppermost regions of the roof. They were sampled adjacent to Eriksfjord crustal xenoliths and were silica-oversaturated (unlike all other syenite variants). A sample with intense late-stage veining (Fig. 4c, d) showed the lowest-δ^{34}S. Sulfides separated from such late-stage veins are marked by exceptionally low-δ^{34}S (down to −15‰, Hutchison et al., 2019), significantly lower than sulfides in early-formed pegmatites and veins (2–4‰, Fig. 4d). Thus, bulk δ^{34}S analyses of Motzfeldt Sø syenites represent mixtures of early-formed syenite with elevated δ^{34}S (greatest in those that have undergone magma-crust interaction) and low-δ^{34}S associated with late-stage cross-cutting veins.

Regional Gardar dykes are classified according to age and setting (Fig. 5a). The dykes are predominantly basaltic, basanitic and tephritic compositions with S concentrations of 20–2300 ppm (Fig. 5a). Two chilled margin samples from Late Gardar dykes in contact with Eriksfjord sandstones show high-δ^{34}S (16–20‰). Comparing the various Gardar dykes (Fig. 5b) we find that Early Gardar dykes emplaced in the Archean (i.e. the most northernly samples) have lowest-δ^{34}S (−1 to 1‰). Two Early Gardar dykes with high-δ^{34}S, overlapping the Late Gardar values, are from basanitic and basaltic-andesite dykes adjacent to the alkaline intrusions (these samples are flagged as blue stars in Fig. 5 and subsequent plots). In Fig. 5b we compare Gardar dyke δ^{34}S to whole-rock and mineral δ^{34}S from lamprophyres and carbonatite diatremes and alkaline intrusions (shown as mean $\pm 1\sigma$).

4.3. Major and trace element trends

A total alkali-silica diagram (Fig. 6) shows Early Gardar dykes are mainly basaltic in composition, while Late Gardar dykes (including chilled margins from the GDC) have slightly lower SiO_2 and higher alkalis which places them in the basanite/tephrite field. Early Gardar dykes spatially associated with alkaline complexes also plot in the basanite/tephrite field.

Considering only the most primitive samples with MgO >4 wt.%, reveals Late Gardar magmas have significantly elevated concentrations of large ion lithophile elements (LILE, e.g. K and Sr), light REE (LREE, La+Ce+Nd) and HFSE (Nb and Ti) compared to Early Gardar magmas (Figs. 7–8). Although these enrichments are not seen in all elements (e.g. heavy REE, Y), parallel trends in LILE and LREE versus MgO provide evidence for distinct initial magmas (Fig. 7). Geochemical differences between Early and Late Gardar are expressed in incompatible trace element ratios (Fig. 9a, b, where one element, Nb or Ce, is more incompatible than the other, Zr or Y). These ratios, i.e. Zr/Nb, Ce/Y and La/Y (not shown), indicate an overall enrichment in incompatible elements in the Late Gardar samples, and suggest different magma sources typify the various dyke generations (Fig. 9b).

Most Gardar melts show depletions in HFSE (Nb and Th) in primitive mantle-normalized trace element plots (Fig. 8). These patterns are characteristic of arc basalts (i.e. mantle sources affected by supra-subduction metasomatism). Moreover, well-established tracers of slab fluid contributions to the mantle wedge

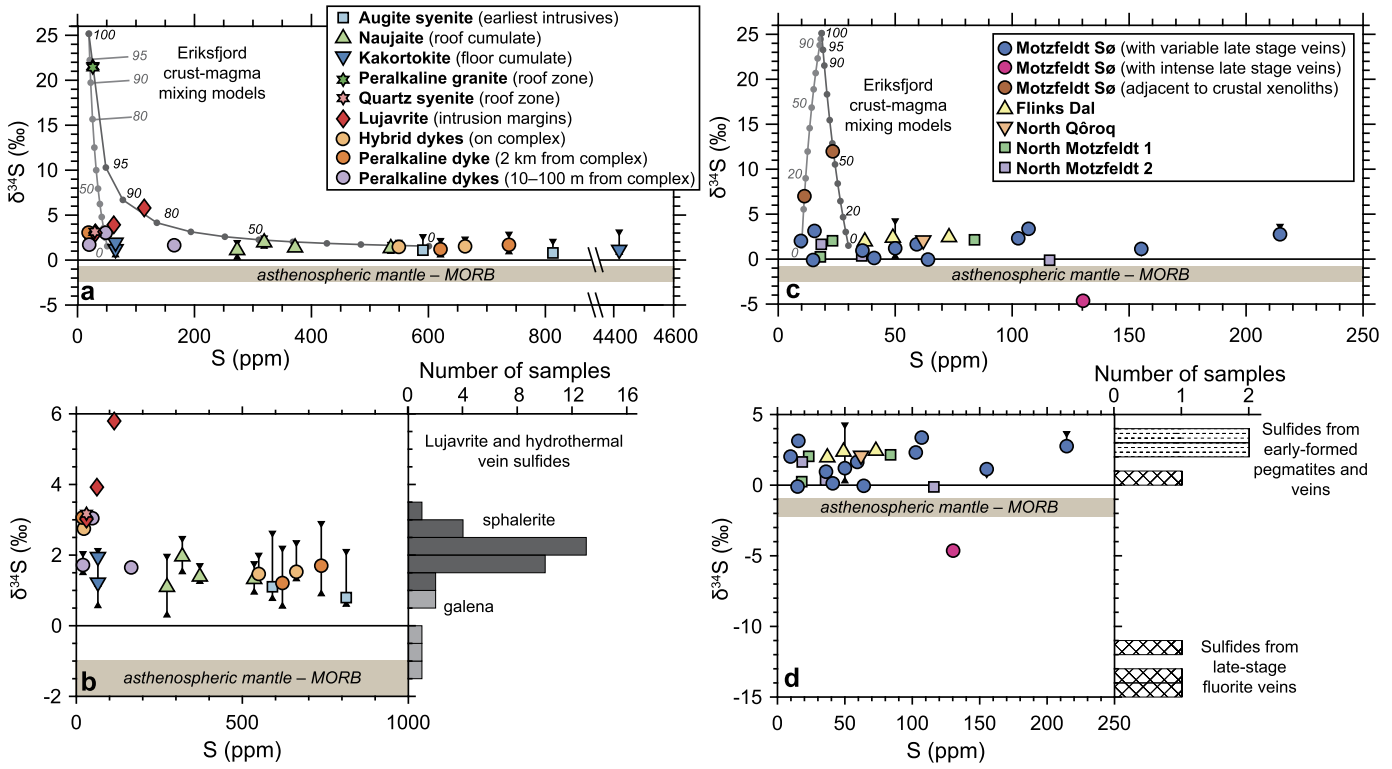

Fig. 4. S concentration and δ^{34}S for the Gardar alkaline complexes. **a)** Overview of whole-rock analyses from Ilímaussaq. Data symbols correspond to the different magmatic units analyzed and a simple description of the sample location is provided in brackets (see Marks and Markl, 2015 for detailed descriptions of each unit). **b)** Ilímaussaq whole-rock analyses compared to a histogram of sulfide mineral δ^{34}S (after Hutchison et al., 2019). **c)** Overview of whole-rock analyses from Motzfeldt. Most of our samples are syenite variants from the mineralized Motzfeldt Sø center (Finch et al., 2019), although data from other magmatic centers are shown. **d)** Motzfeldt whole-rock analyses compared to a histogram of sulfide mineral δ^{34}S. Note the histogram distinguishes early- versus late-stage sulfides (shown by the dashed line and hatched fills, respectively). In **a)** and **c)** a binary mixing model is used to examine contamination of a primitive Gardar melt (with $\delta^{34}S = 1.5‰$, and variable S concentration) with Eriksfjord sandstone (with $\delta^{34}S = 25‰$ and S = 19 ppm, the average of multiple analyses, Supplementary Data 1). Initial S concentrations are 600 and 50 ppm for Ilímaussaq, and 30 and 10 ppm for Motzfeldt (see further details in Supplementary Information). For samples with distinguishable acid volatile phases a black vertical line connects the δ^{34}S of their acid volatile sulfur (AVS, downward pointing triangle) and chromium reducible sulfur (CRS, upward pointing triangle). The beige horizontal bar indicates the δ^{34}S of the asthenospheric mantle (MORB sources, after Labidi et al., 2013).

(i.e. Ba/La, Carr et al., 1990), show that Gardar magmas have values comparable to those of modern subduction zones (20–50, Carr et al., 1990; Kelemen et al., 2003) and subduction-influenced rifts (10–40, Rooney and Deering, 2014). Halogen concentrations are also comparable to subduction zones (e.g. F, Fig. 9d), and show greatest enrichment in Late Gardar dykes and those Early Gardar dykes spatially associated with alkaline complexes (Fig. 1c, Köhler et al., 2009).

In addition to the gross geochemical distinctions between Early and Late Gardar we note:

1) The Late Gardar OGDC and YGDC show comparable trace element enrichment (Fig. 8), Zr/Nb and Ce/Y (Fig. 9b) to the Tuttutooq–Ilimmaasaq–Narsarsuaq dyke swarm,
2) The Late Gardar Nunarsuit–Isortoq dyke swarm shows greatest geochemical affinity to the Early Gardar dykes (Figs. 8, 9),
3) The Eriksfjord lavas suggest geochemical kinship to Early Gardar dykes (Fig. 7), although a few samples are enriched in Ti, P, Sr and LREE and overlap values of the Late Gardar dykes.
4) Several Early Gardar dykes adjacent to alkaline complexes show selective enrichment in LREE and HFSE and overlap Late Gardar dykes values (Figs. 8, 9a, b),
5) Lamprophyres have the greatest concentrations of LILE, HFSE and REE (Fig. 8). Unlike all other Gardar melts their trace element patterns (Fig. 8) do not display negative Th and Nb anomalies and are more akin to asthenospheric OIB-type sources,
6) Incompatible element ratios for Motzfeldt, Ilímaussaq and Ivigtût (Fig. 9a, b) are comparable to those found in the Late Gardar dykes.

5. Discussion

5.1. Sulfur isotope insights into Gardar magmatic processes: giant dykes and alkaline complexes

Gardar giant dykes and alkaline complexes represent large upper-crustal magmatic systems. These samples show no relationship between δ^{34}S and S concentration (Figs. 3–4) and do not support extensive S degassing (cf. Fig. 2b). This is consistent with their emplacement at 3–4 km (~100 MPa, Upton et al., 2003; Krumrei et al., 2007) which precludes extensive S degassing (Aiuppa et al., 2007), and their peralkaline melt composition which have higher S solubilities than other silicate magmas (Scaillet and MacDonald, 2006).

The late Gardar OGDC and YGDC are basaltic-basanitic magmatic intrusions that underwent significant fractional crystallization to yield a range of gabbroic to syenitic units (Upton, 2013). Given the importance of crystal fractionation, we compare their δ^{34}S to models of sulfide mineral fractionation (Fig. 3). For the OGDC, we use our sample from the chilled margin as a parental composition. For the YGDC, we did not make new S concentration and δ^{34}S analyses of the chilled margin and instead use S concentration measurements from Upton and Thomas (1980) and averaged the δ^{34}S of contemporaneous Late Gardar dykes adjacent

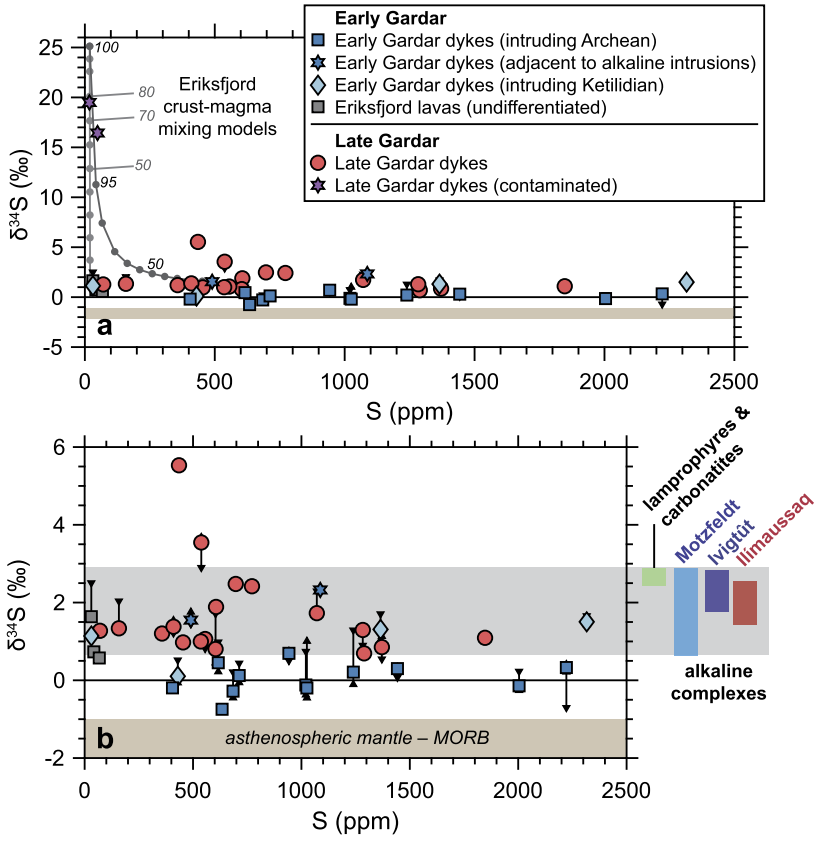

Fig. 5. S concentration and δ^{34}S for Gardar regional dykes and Eriksfjord lavas. **a)** Overview of all whole-rock analyses. Two Late Gardar dykes in contact with Eriksfjord sediments show extremely elevated δ^{34}S (16–20‰) and a binary mixing model is used to examine magma-crust interactions. Lines show end-member mixing between a primitive Gardar melts (with $\delta^{34}S = 1.5$‰, and initial S concentrations of 500 and 20 ppm) and Eriksfjord sandstone (with $\delta^{34}S = 25$‰ and S = 19 ppm, the average of multiple analyses, Supplementary Information). **b)** Detailed comparison of dyke and lava δ^{34}S analyses with values from lamprophyre and carbonatite diatremes (after Hutchison et al., 2019) and Gardar alkaline intrusions (Motzfeldt, Ivigtût and Ilímaussaq, after this study and Hutchison et al., 2019, shown as mean $\pm 1\sigma$). As in previous S isotope plots, those samples with distinguishable acid volatile sulfur (AVS) phases are shown by a black vertical line connecting the δ^{34}S of their AVS (downward pointing triangle) and chromium reducible sulfur (CRS, upward pointing triangle). The grey shaded region in the middle of the plot shows the range of δ^{34}S in Gardar alkaline intrusion and diatremes, while the lower beige bar shows the δ^{34}S of the asthenospheric mantle (Labidi et al., 2013).

to the YGDC. Fig. 3 shows that neither dyke perfectly matches a silicate melt or segregated FeS (cumulate) δ^{34}S evolution. This implies that S systematics of the giant dykes have characteristics of both melt and cumulate systems. This seems reasonable because although the dykes were emplaced as a single melt intrusion, various segments of the dykes show modal layering and clear evidence of cumulate processes. Their magmatic textures also evidence a melt-mush body with well-developed intercumulus melt phases (Upton, 2013).

Although models of sulfide fractionation explain the overall S systematics of the giant dykes an interesting observation is that while evolved (syenitic) rocks of the OGDC show lower S concentrations and bulk δ^{34}S than their associated gabbros, the opposite is true for the YGDC (Fig. 3). An explanation for this difference in S systematics is that OGDC syenites are representative of a melt composition, while YGDC syenites are representative of a cumulate composition. Cu contents provide an insight into sulfide mineral content of the syenites, and data from Upton et al. (1985) and Upton and Thomas (1980) show these are ~3 ppm and ~20 ppm, in the OGDC and YGDC syenites, respectively. This supports greater sulfide removal in the OGDC syenites, and/or greater sulfide accumulation in the YGDC syenites. Ultimately, these variations in syenite S systematics highlight the complexities of sulfide mineral fractionation in large melt-mush bodies. More samples and a detailed petrographic investigation (with high-spatial resolution S isotope data) are necessary to examine these processes thoroughly.

Ilímaussaq and Motzfeldt are two of the largest alkaline complexes and host significant REE and HFSE deposits. At Ilímaussaq, bulk δ^{34}S is remarkably uniform (Fig. 4b); nepheline syenitic roof and floor cumulate which have a vertical separation of >1 km are indistinguishable, as are different peralkaline dykes sampled at 10–100 m and ~2 km from the complex. δ^{34}S of the earliest Ilímaussaq rocks (augite syenites) overlap values of final stage lujavrite and hydrothermal veins (Fig. 4b) indicating that fractional crystallization had a negligible impact on melt δ^{34}S. Closed-system sulfide mineral fractionation (Fig. 2b) generates ≤1‰ variations in δ^{34}S and would be difficult to detect given the natural ±0.4‰ heterogeneity in our samples. Previous geochemical studies of Ilímaussaq support a largely closed-system evolution (Marks et al., 2004), and our models of sulfide segregation account for the variations in S concentration and negligible δ^{34}S change.

Motzfeldt shows similar positive δ^{34}S (Fig. 4c). However, a key difference between Ilímaussaq and Motzfeldt Sø syenites is that the latter have undergone intense late-stage hydrothermal alteration and oxidation (Finch et al., 2019). The Motzfeldt Sø roof-zone samples are brick-red in color and cross-cut by late-stage veins (rich in fluorite, sulfide and sulfate, Hutchison et al., 2019). Sulfides separated from these late-stage veins show extremely low-δ^{34}S (down to −15‰). Our analytical procedure only extracts sulfide phases, so the bulk δ^{34}S for Motzfeldt Sø samples represent mixtures of early-formed sulfides in the syenite matrix (with slightly elevated δ^{34}S) and late-stage sulfides in cross-cutting veins (with

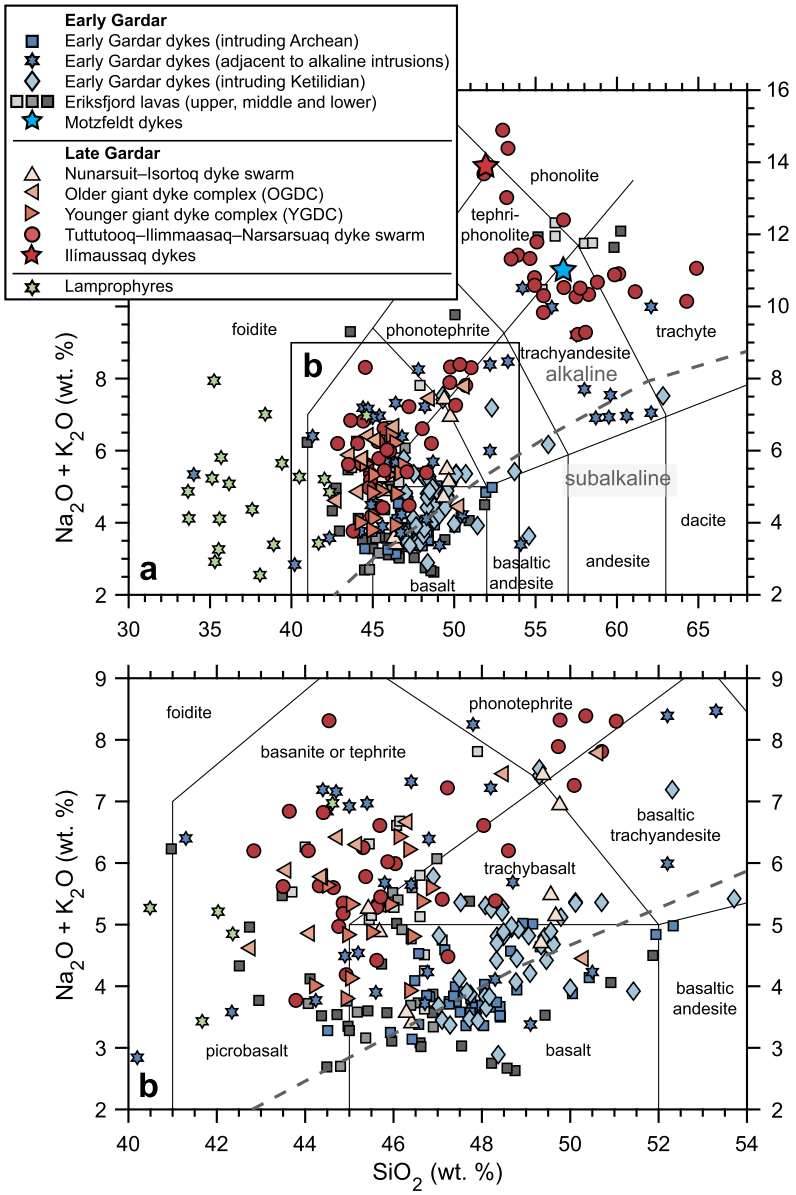

Fig. 6. Total alkalis versus silica (TAS) diagram showing whole-rock analyses of Gardar dyke swarms and lavas. Gardar magmatism falls in two distinct periods, 1320–1260 Ma and 1180–1140 Ma, referred to as Early and Late Gardar, respectively. Note that lamprophyres occur in both magmatic periods (Upton, 2013). The grey dashed line shows the alkaline sub-alkaline (tholeiitic) divide of Irvine and Baragar (1971). Note that average melt compositions are also shown for alkaline complexes Ilímaussaq and Motzfeldt (large stars). Ilímaussaq dyke compositions are from analyses of peralkaline phonolite (micro-kakortokite) dykes injected into the surrounding country rock (Larsen and Steenfelt, 1974), while those for Motzfeldt are from unaltered microsyenite dykes in the Motzfeldt Sø center (Finch et al., 2019).

low-δ^{34}S). This mixing is expressed in the most altered roof-zone sample with δ^{34}S of -5‰ (Fig. 4d).

Samples from the roof and margins of the complexes suggest crustal interactions. Since δ^{34}S in the most contaminated samples (Fig. 4) is greater than δ^{34}S in Ketilidian or Archean crust, the only credible contaminant is Eriksfjord sandstone. At Ilímaussaq, peralkaline granites from the roof zone dominantly comprise alkali feldspar and quartz, plus ~15% alkali pyroxene and amphibole. Their petrogenesis remains obscure; while δ^{18}O analyses of amphibole separates show typical magmatic values, Nd isotopes and δ^{18}O of quartz and feldspar suggest origins through crustal contamination (Stevenson et al., 1997; Marks et al., 2004). δ^{34}S data reveal that the high-δ^{34}S of the peralkaline granite closely resembles the high-δ^{34}S Eriksfjord sandstone in the roof (Section 4.1). We suggest these peralkaline granites represent a complex interaction between a peralkaline melt/fluid, and the local Eriksfjord sandstone roof. Alkali minerals (pyroxene and amphiboles) exhibit typical magmatic δ^{18}O, while other phases such as quartz, feldspar and sulfides show crustal δ^{18}O and δ^{34}S signatures.

Lujavrites from the margin of Ilímaussaq, adjacent to Eriksfjord xenoliths, show slightly greater bulk δ^{34}S than sulfide minerals separated from xenolith-free lujavrites (Fig. 4b). To explain this we invoke interactions with high-δ^{34}S Eriksfjord crust (consistent with previous Nd isotopic investigations of similar samples, Stevenson et al., 1997). Finally, at Motzfeldt, δ^{34}S data also fingerprint a high-δ^{34}S contaminant in the upper-most silica-oversaturated syenites, which can only plausibly be linked to the Eriksfjord sandstones.

5.2. *The sulfur isotope signature of the Gardar mantle: insights from regional dyke swarms*

Crustal contamination, sulfide fractionation and hydrothermal overprint modify S isotopes in the giant dykes and alkaline com-

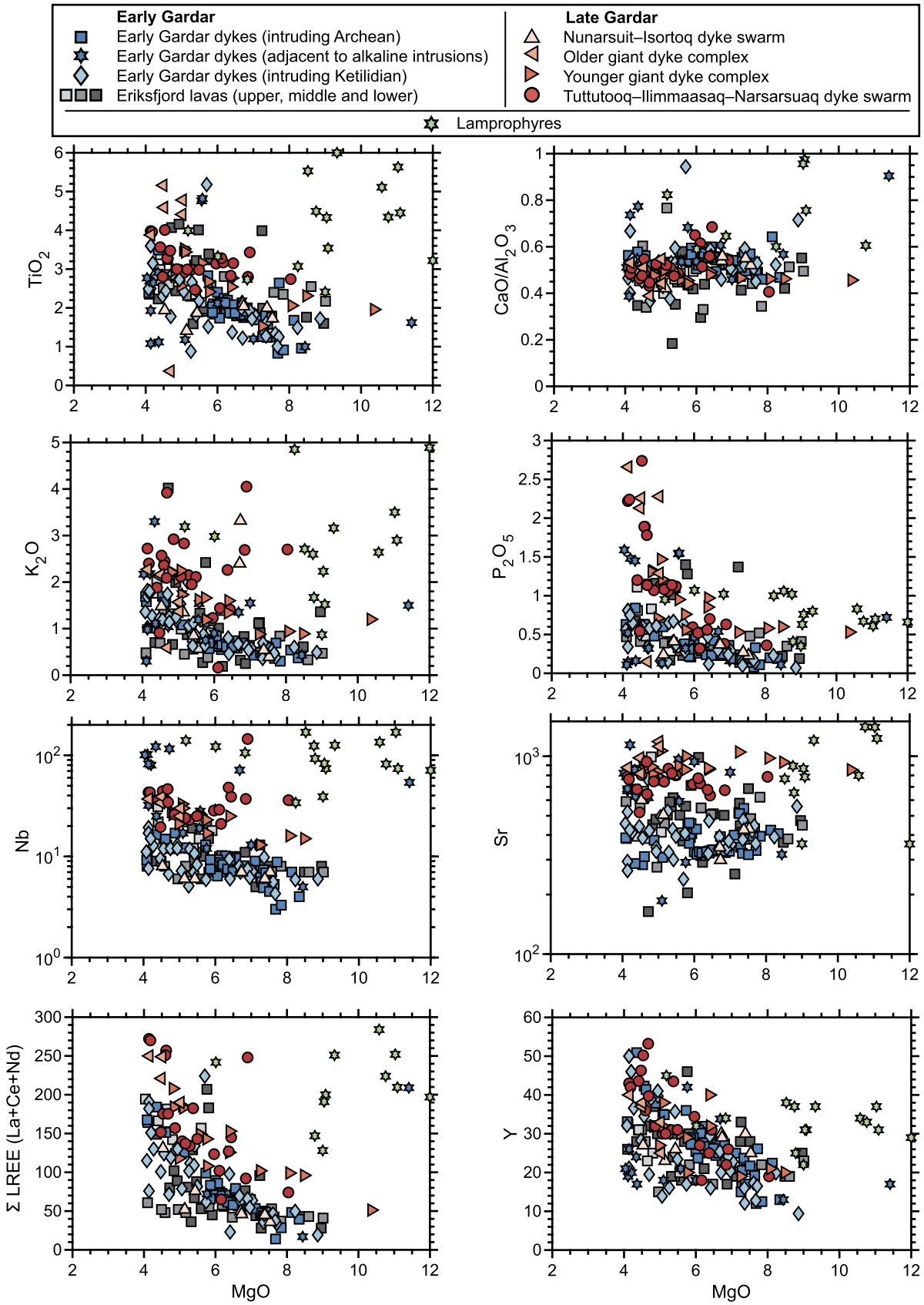

Fig. 7. Selected major and trace elements versus MgO for the Gardar dyke swarms and lavas. Only primitive samples with MgO >4 wt.% are shown. Note that lamprophyres occur in both Early and Late Gardar periods (Upton, 2013).

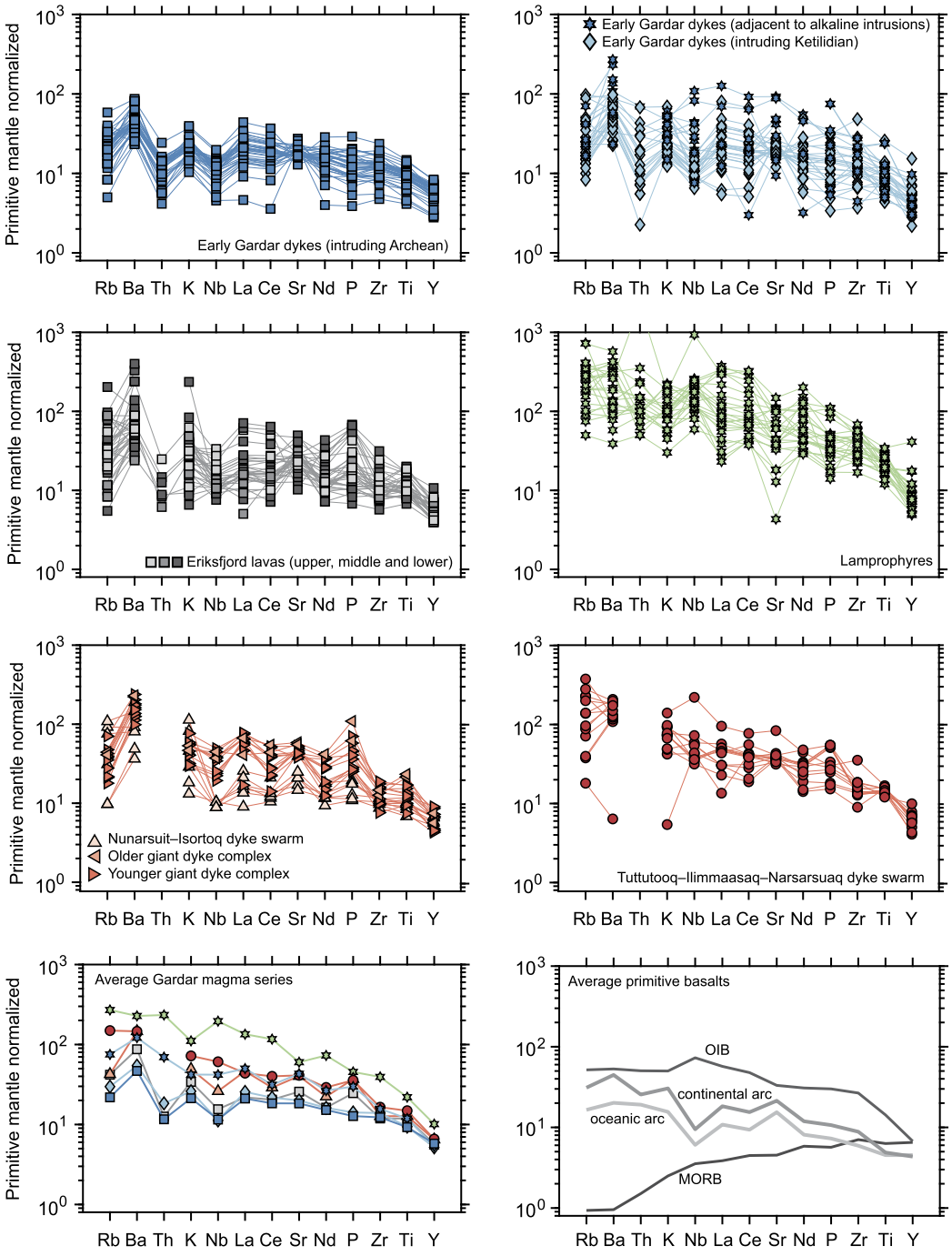

Fig. 8. Primitive mantle-normalized (Sun and McDonough, 1989) trace element diagram showing the various suites of Gardar dykes and lavas. To reduce overlapping data and improve readability only primitive samples with >5 wt.% MgO are plotted. Note that no Th data was available for the Late Gardar dykes and the Th concentration of the lamprophyre sample which plots above the vertical axis is 2240 ppm. In the lower left we show the average values of each magma series. Note that in the average plot all values for Eriksfjord lavas (upper, middle and lower) have been taken together (shown by the light grey squares), as have the values for the Nunarsuit–Isortoq dyke swarm and Older and Younger giant dyke complexes (shown by the pink triangles). Also shown are average compositions of mid-ocean ridge basalts (MORB), oceanic island basalts (OIB), continental arc basalts and oceanic arcs basalts (after Sun and McDonough, 1989 and Kelemen et al., 2003).

plexes. These processes are only observed in a few samples and, the most primitive samples all show $\delta^{34}S$ of 0–4‰, making them enriched in ^{34}S with respect to the upper mantle (-1 ± 0.5‰, Labidi et al., 2013).

To avoid these issues, we investigated mafic dyke swarms (Fig. 5). Their fine-grained homogeneous textures and small volume (most are only 1–20 m wide) indicate rapid cooling and short crustal residence. An assessment of S isotope modification is still required, and our analysis of the chilled margins of two dykes in contact with high-$\delta^{34}S$ Eriksfjord sediments emphasizes the potential for contamination in those with low S contents ($\leq$100 ppm, Fig. 5a). We stress that dykes in contact with Eriksfjord sediments occur in a small area of the province (Fig. 1). Most are sufficiently S-rich (300–2400 ppm) that we can discount this process (Section 4.1). There is no evidence for degassing trends (cf. Fig. 2b), and so we suggest sulfide segregation governs S concentration but has negligible impact on melt $\delta^{34}S$.

It follows that the mafic dykes associated with Gardar magmatism provide accurate constraints on mantle $\delta^{34}S$. Although Gardar dykes have primitive compositions (Fig. 6) they show surprisingly

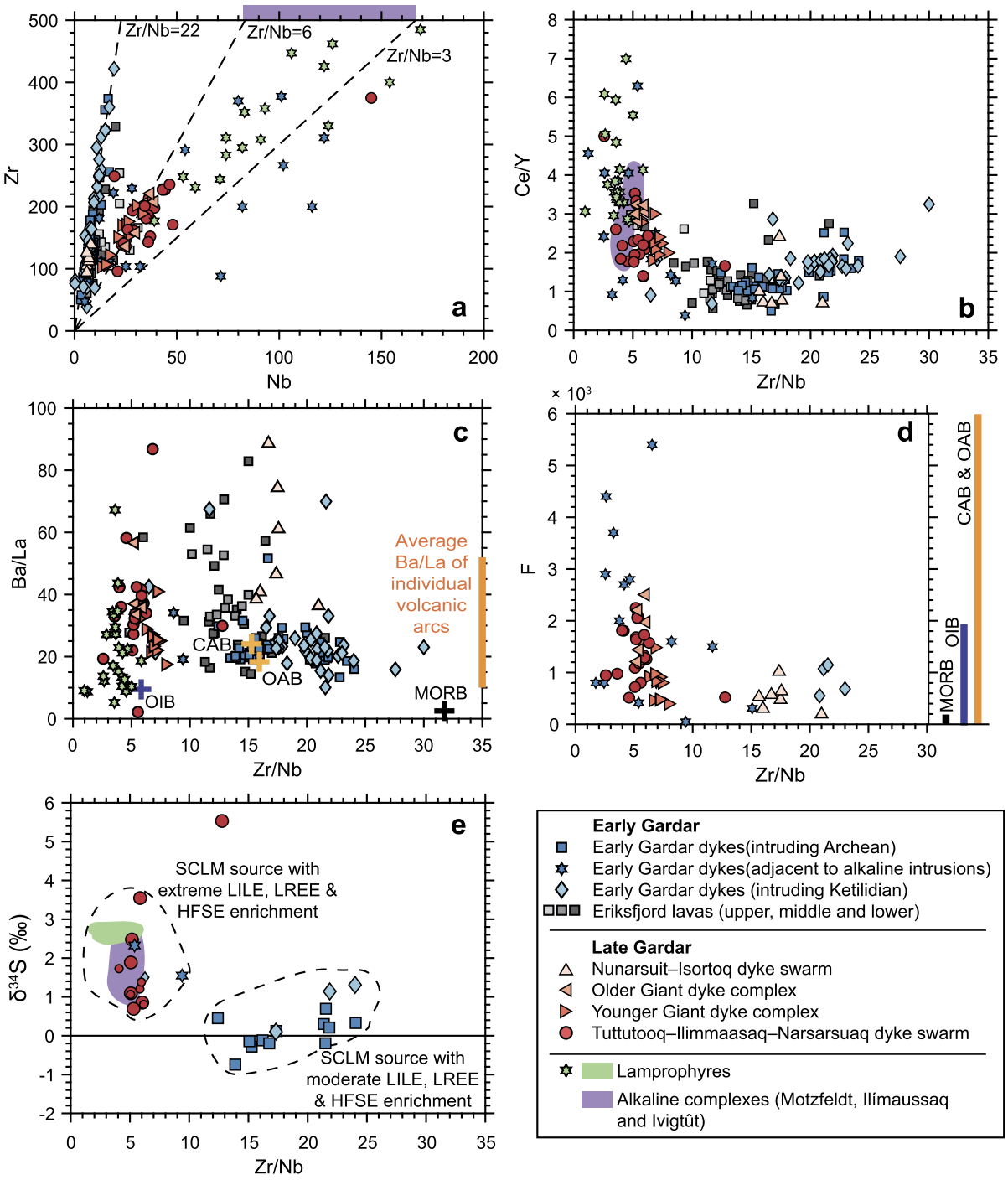

Fig. 9. Incompatible element ratios and $\delta^{34}S$ for the various Gardar magmatic suites. In a–d only samples with MgO >4 wt.% are shown, in e the smaller symbols identify those samples with MgO <4 wt.%. Geochemical variations in the various Gardar magmatic suites are most clearly observed in incompatible trace element ratios (where one element, Nb or Ce, is more incompatible than the other, Zr or Y). In c, crosses show average values for mid-ocean ridge basalts (MORB), oceanic island basalts (OIB), continental arc basalts (CAB) and oceanic arcs basalts (OAB) after Sun and McDonough (1989) and Kelemen et al. (2003). Average Ba/La from individual volcanic arcs (cf. Kelemen et al., 2003) show values up to 50, overlapping most of the Gardar data, and are shown by the orange bar. In d, the range of F contents in MORB and OIB follow compilations of Hanley and Koga (2018) while the arc basalt range (CAB and OAB) is from the compilation of Van Den Bleeken and Koga (2015). Note that Gardar F data are relatively limited and unavailable for several Gardar magmatic suites (e.g. the Early Gardar dykes intruding the Archean). Also note the abbreviation SCLM: sub-continental lithospheric mantle.

high-$\delta^{34}S$ (Fig. 5b). Since $\delta^{34}S$ is unaffected by mantle partial melting (Labidi and Cartigny, 2016) these values indicate genuine ^{34}S enrichment of the Gardar mantle. The dykes also show a wide range of $\delta^{34}S$ (−1 to 6‰, Fig. 5), suggesting considerable heterogeneity at source, and subtle but discernible $\delta^{34}S$ variation between dyke swarms. Early Gardar dykes in the Archean crust, are on average ~1‰ lower than Late Gardar dykes in Ketilidian crust (Fig. 1). Notably, there are rare examples of Early Gardar dykes with enriched $\delta^{34}S$ found in the Archean crust (Fig. 5), but unlike the rest of the dyke swarm, these are only found adjacent to the alkaline intrusions. This precludes a straightforward time-evolution in $\delta^{34}S$ between Early and Late Gardar.

Finally, comparing dyke $\delta^{34}S$ to other magmas from the Gardar province reveals significant overlap between the Late Gardar dykes,

the alkaline complexes (Motzfeldt, Ivigtût and Ilímaussaq) and primitive lamprophyric and carbonatitic diatremes (Fig. 5b). The latter are pertinent to the discussion of mantle sources because Upton (1991) showed that Gardar lamprophyres contain fragments of altered mantle xenoliths (discussed below). Thus, lamprophyres provide direct constraints on the $\delta^{34}S$ of the Gardar mantle (Coulson et al., 2003) and their high values also support an overall ^{34}S enrichment of the source (Fig. 5b).

5.3. Mantle source enrichment and the origins of Gardar magmas

Enriched $\delta^{34}S$ signatures typify all Gardar magmas and require a component of recycled surface S (with positive $\delta^{34}S$) in the Gardar mantle. Additional insights into Gardar mantle sources come from our major and trace element compilation. We note crustal contamination is a potential issue when interpreting such data, but stress that previous publications on these samples demonstrated minor crustal interactions (0–20%, Köhler et al., 2009; Bartels et al., 2015). For brevity, we avoid repeating these arguments here.

Geochemical investigations of Gardar dykes have previously suggested REE- and HFSE-enriched mantle sources and linked these to plume activity (OIB-type sources, Halama et al., 2003) or metasomatism of the sub-continental lithospheric mantle (SCLM, Bartels et al., 2015). Our compilation supports the latter hypothesis. For example, the characteristic depletions in HFSE (Nb and Th in Fig. 8) are analogous to arc basalts not OIB. Moreover, Ba/La (Fig. 9c), which traces slab fluid contributions to the mantle wedge, is significantly elevated above OIB, being comparable to modern subduction zones and subduction-influenced rifts (10–50, Carr et al., 1990; Kelemen et al., 2003; Rooney and Deering, 2014).

The only samples not showing signatures of a subduction-influenced source are lamprophyres. Although lamprophyres are rare, they lack Nb and Th anomalies (Fig. 8) and show low Ba/La and Zr/Nb (Fig. 9c) reminiscent of asthenospheric OIB-type sources. Radiogenic isotopes have previously suggested a distinct source for these lamprophyres (Goodenough et al., 2002; Upton et al., 2003), and we also find that their $(Gd/Yb)_N$ values (2–6), are higher than all other Gardar melts (1.4–2) and indicative of garnet in the source. In short, although lamprophyre $\delta^{34}S$ is comparable to other Gardar magmas, and requires a component of recycled surface S, their trace elements indicate a distinct, deeper origin, and a principal hypothesis is that these lamprophyres represent small-degree melts of an asthenospheric source which became frozen in as metasomes in the SCLM during initiation of the Gardar and re-melted during rifting (Goodenough et al., 2002).

Widespread metasomatism of the Gardar lithospheric mantle is logically linked to a period of Andean-style subduction which took place in the Ketilidian (Fig. 1b). Although the precise source of the enriched $\delta^{34}S$ signature is difficult to determine, high-$\delta^{34}S$ candidates are: seawater sulfate released by the slab (Wallace and Edmonds, 2011); recycled Proterozoic sediments (Labidi et al., 2015) and/or serpentinized oceanic peridotites (Alt et al., 2013). We suggest that high ^{34}S slab fluids and melts percolated through existing peridotitic mantle and formed metasomatic veins which sequestered HFSE, REE, alkalis and halogens in minerals such as apatite, phlogopite and/or amphibole (Köhler et al., 2009). Importantly, apatite and phlogopite have been observed in metasomatized peridotitic mantle xenoliths entrained in Gardar lamprophyres (Upton, 1991). Bartels et al. (2015) suggested the presence of amphibole based on negative Hf anomalies in Early Gardar dykes. Although amphibole has not been observed in mantle xenoliths its inferred presence strongly supports a lithospheric source (since mantle amphiboles are stable at temperatures $<1150\,^{\circ}C$, Mandler and Grove, 2016). In summary, multiple lines of evidence support widespread metasomatism of the lithospheric mantle during Ketilidian subduction. This enriched the Gardar source in slab-derived metals, alkalis, and volatiles (Figs. 6, 7, 8, 9d).

Early and Late Gardar dykes have distinct $\delta^{34}S$ (Fig. 5b), and these are also expressed in their major and trace elements (Figs. 6–9). Plots of CaO/Al_2O_3 versus MgO (Fig. 7) show little difference between Gardar magmatic suites suggesting little variation in the main fractionating assemblage. Therefore, differences in geochemical enrichment reflect variation in source lithology and/or melting processes. S isotopes provide a crucial insight: because $\delta^{34}S$ is unaffected by mantle partial melting (Labidi and Cartigny, 2016), Gardar $\delta^{34}S$ variations must reflect genuine compositional variability in mantle sources; dykes with highest-$\delta^{34}S$ have the greatest component of recycled surface S in their source. These signatures are found in both Late Gardar dykes and those Early Gardar dykes spatially associated with alkaline complexes (Fig. 5b). High-$\delta^{34}S$ dykes also show the strongest subduction fluid imprint (Fig. 9c) and are enriched in the most incompatible trace elements (Fig. 9a–d). This indicates that mantle sources for high-$\delta^{34}S$ Gardar magmas are particularly enriched in REE, HFSE, alkalis, and halogens, and the metasomatic phases that host these elements. Thus, alkaline complexes are spatially associated with high-$\delta^{34}S$ enriched mantle sources. Occurrence of mineralized complexes in both phases of Gardar magmatism demonstrates that enriched mantle domains existed prior to rifting and were tapped throughout.

The Gardar is notable for its episodic magmatism, and the southward shift and focusing of rifting during the Late Gardar (Upton, 2013). We identify two additional features: 1) a large-scale lateral variation in metasomatic enrichment (Early Gardar dykes intruding the Archean, i.e. the most northerly dykes, have the lowest-$\delta^{34}S$, Fig. 5b, and the weakest subduction imprint), and 2) the existence of metasomatically-enriched domains throughout the Gardar lithospheric mantle and recurrence of these mantle signatures in both phases of magmatism.

To reconcile these observations, we suggest Gardar mantle heterogeneity is intimately linked to supra-subduction zone processes (Fig. 10). During Ketilidian subduction, fluids and melts released from the descending slab metasomatized the mantle wedge and enriched the whole mantle in LREE, HFSE, alkalis and volatiles (including, $\delta^{34}S$). Studies of modern subduction zones consistently find evidence for down-slab variation in both the flux and composition of the slab fluids and melts (Watt et al., 2013) as the pressure-temperature threshold of different hydrous minerals are exceeded (Grove et al., 2012). Much of the slab dehydration occurs beneath the arc-front and fore-arc (Ribeiro et al., 2015), and experimental studies demonstrate that these aqueous fluids are highly efficient at mobilizing REE from the slab (Tsay et al., 2014). At greater depths, wet melting of slab sediments and mafic crust becomes significant, and numerical models suggest localized pulses of wet melting (and hence REE release) occur down-slab (van Keken et al., 2011). In the context of the Gardar, where the slab was descending in a northward direction (Fig. 1b), these processes account for the overall decrease in metasomatic signature (low-$\delta^{34}S$) in the northernly Archean craton and localized REE-enriched domains with high-$\delta^{34}S$ (Fig. 10a). Importantly, down-slab variation in fluid release suggests lateral mantle heterogeneities on a scale of 10–50 km (van Keken et al., 2011) consistent with the lateral variation in dyke $\delta^{34}S$ observed at the surface. In the Early Gardar (Fig. 10b), magmatism was widespread and although it predominantly tapped moderately enriched lithospheric sources, alkaline complexes and their adjacent primitive dykes originate from localized mantle domains enriched in LREE, HFSE, alkalis and volatiles (Figs. 6b, 7, 9d). In the Late Gardar (Fig. 10c), rifting was focused in two magmatic segments in the Ketilidian crust in the south of the province. The magma source for the more southerly Tuttutooq-Ilimmaasaq-Narsarsuaq zone was

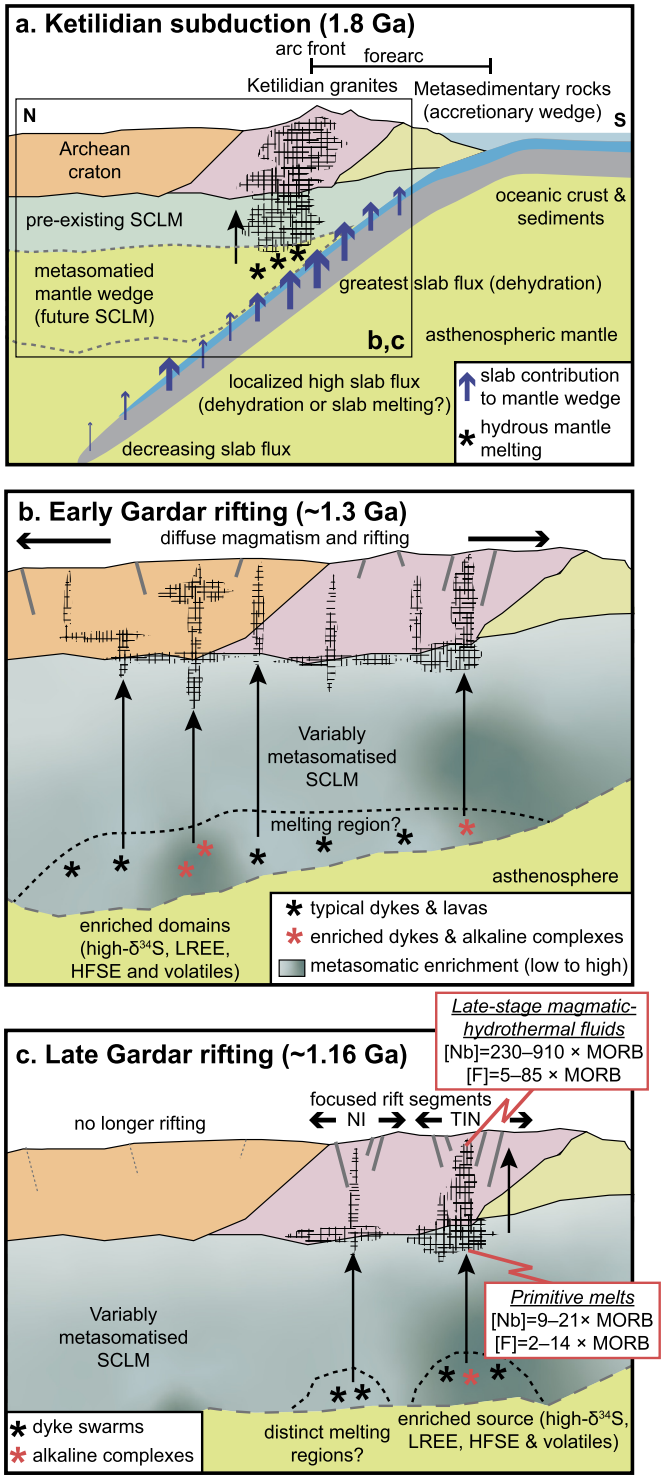

in closer proximity to the palaeo-arc-front and accessed a more intensely metasomatized and enriched mantle source. The dykes from the more northerly Nunarsuit–Isortoq swarm show geochemical kinship to Early Gardar dykes, suggesting an only moderately enriched source.

Our model accounts for both the regional and localized subduction-related metasomatism observed in the Gardar dykes and suggests that recurrence of alkaline complexes over ~200 Ma of rifting reflects the repeated tapping of enriched high-δ^{34}S lithospheric mantle sources. One uncertainty is whether the relative contribution of asthenospheric versus lithospheric mantle sources changed significantly between Early and Late Gardar. Although we cannot uniquely fingerprint these different mantle endmembers, we underscore that all Gardar dykes show strong subduction zone signatures (Figs. 8, 9c), and that trace element systematics for Late Gardar Nunarsuit–Isortoq dykes and Early Gardar dykes are almost identical (despite melting regimes likely being different, Fig. 10b,c). This argues for a dominant lithospheric mantle component in all Gardar melts (Bartels et al., 2015), and supports experimental studies (Pilet et al., 2008) which show that melting mixtures of peridotite plus hydrous metasomatic phases, analogous to Gardar lithospheric mantle, generate a melt dominated by the metasomatic phases with a negligible contribution from the peridotite.

5.4. Insights into the mantle source of world-class REE and HFSE resources

We have demonstrated that mineralized alkaline complexes originate from mantle sources enriched in REE, HFSE, alkalis and volatiles. This raises several questions. Firstly, are similar patterns of source enrichment observed at other alkaline provinces? A useful comparison is the Devonian Kola Alkaline Province, which hosts some of the world's largest REE and HFSE deposits in nepheline syenites and carbonatites. Like the Gardar, there is strong geochemical evidence that Kola alkaline complexes derive from a mantle source that was intensely metasomatized shortly before the onset of magmatism (Kogarko et al., 2010). However, mantle metasomatism in Kola has been linked to a mantle plume rather than prior subduction. OIB-type signatures are expressed in trace element data (Supplementary Information), although it is unclear whether Kola melts derive from metasomatized asthenospheric and/or lithospheric sources (Downes et al., 2005). In any case, the most primitive melts feeding the Kola alkaline complexes all show strong LREE and HFSE enrichment (Downes et al., 2005). In contrast, contemporaneous basaltic dyke swarms, spatially distanced from alkaline complexes, show limited evidence for REE and HFSE enrichment and originate from a largely unmetasomatized mantle source (Arzamastsev et al., 2017). Thus, there is good evidence that mantle domains associated with Kola alkaline complexes experienced greatest metasomatism and enrichment in REE,

Fig. 10. Summary of mantle enrichment and magmatic evolution in the Gardar Province. **a)** shows Andean-style subduction during the Ketilidian orogeny. Subduction releases slab fluids and melts which cause metasomatism of the mantle wedge enriching it with LILE, LREE & HFSE, and an overall high-δ^{34}S. During active subduction, slab dehydration is greatest beneath the arc-front and fore arc and triggers hydrous melting of the mantle wedge (leading to the Ketilidian granites). The slab contribution to the wedge (i.e. slab melt plus fluid) decreases as it descends (shown by blue arrows). However, there are likely to be significant variations down-slab as changes in pressure and temperatures cause different minerals to breakdown and facilitate localized wet melting of the slab (van Keken et al., 2011; Watt et al., 2013). This leads to heterogeneous enrichment of the sub-continental lithospheric mantle (SCLM) but with an overall northward decrease in metasomatic signature (shown by the intensity of the green colors in b and c). In the Early Gardar **(b)** magmatism is widespread and intrudes both Archean and Ketilidian crust. All Early Gardar dykes show an enriched subduction zone signature (which originates from the metasomatized SCLM) but this is particularly pronounced in melts that are spatially associated with the alkaline complexes (these show the highest-δ^{34}S, LREE, HFSE and halogen contents). We suggest these enriched mantle domains are the result of prior subduction and the varying slab input shown in a. In the Late Gardar **(c)** focused magmatism occurs in the Nunarsuit–Isortoq (NI) and Tuttutooq–Ilimmaasaq–Narsarsuaq (TIN) magmatic segments (located in the NW and SE of the Ketilidian crust, respectively). The Tuttutooq–Ilimmaasaq–Narsarsuaq magmas show extreme enrichment in δ^{34}S, LREE, HFSE and halogens and derive from a more enriched lithospheric mantle source (we suggest this reflects its proximity to the paleo-arc-front and the zone of greatest slab input, shown in a). The Nunarsuit–Isortoq magmas are sourced from less enriched mantle and show geochemical affinity to Early Gardar dykes (indicating a similar SCLM source). Note that in all plots the black hatched region shows the approximate extent of magma plumbing system while vertical black lines show magma ascent from the mantle source. In b and c horizontal arrows show extension while solid grey lines show normal faulting.

HFSE and volatiles. This is coherent with our findings and suggests that plume- and subduction-related metasomatism generate enriched mantle domains that form the source of large, mineralized alkaline intrusions.

This raises a further question: is source enrichment critical for generating world class alkaline igneous deposits? In response, we determine how a typical, economically important HFSE (e.g., Nb) varies in concentration from its primitive mantle source to its final emplacement as a mineralized magmatic-hydrothermal fluid in an alkaline intrusion. Late Gardar dykes of the Tuttutooq-Ilimmaasaq-Narsarsuaq zone and those Early Gardar dykes spatially associated with alkaline centers provide the best constraints on the primary melts that feed mineralized alkaline complexes. Their average Nb concentrations are ~35 ppm which is 7× greater than typical arc basalts and 15× greater than MORB (Fig. 10c). Thus, subduction zone metasomatism and subsequent low-degree melting of the enriched Gardar mantle generate primitive melts with HFSE contents ~15 times higher than typical asthenospheric magmas. These enriched melts were then delivered to large upper-crustal magma bodies (e.g. Motzfeldt and Ilímaussaq) where they underwent extended fractional crystallization. Whole-rock analyses of the most chemically evolved units have Nb concentrations of 500–2000 ppm (Sørrensen, 1992). Thus, magmatic fractionation and hydrothermal processes are responsible for a 100–1000× increase in the initial HFSE content. This emphasizes that the greatest absolute increase in HFSE concentration occurs during magmatic processing rather than mantle source enrichment (Fig. 10c).

Although this may suggest a relatively insignificant role for the mantle source in the genesis of alkaline igneous deposits, we emphasize that enriched mantle domains also generate melts with high concentrations of alkali and volatile elements (Figs. 6b, 9d). These species (Na, K, F, Cl, S) play an essential role in the formation of alkaline igneous complexes by maintaining the solubility of HFSE in the melt throughout fractionation, depressing solidus temperatures and allowing extended fractionation, and, in alkaline fluids, acting as ligands to complex HFSE and locally concentrate these in the final stages of crystallization (Kogarko, 1990; Anenburg et al., 2020). We suggest the co-location of REE, HFSE, alkalis and volatiles in high concentrations in the mantle source is critical to the formation of these mineralized alkaline complexes; these elements are incompatible during mantle melting (Schilling et al., 1980), and during transport through the crust, volatiles and alkalis play a critical role in amplifying REE and HFSE contents of the residual melt/fluid. In summary, although magmatic and hydrothermal processes, rather than source enrichment, account for the greatest absolute increase in REE and HFSE content, the unique combination of the rare metals plus the melt-modifying and metal-transporting alkalis and volatiles in the primary melts that feed alkaline complexes is critical to the formation of world-class alkaline igneous deposits.

6. Conclusions

New S isotope analyses and a compilation of major and trace element data shed light on the mantle origin and magmatic evolution of alkaline magmas in Greenland's Gardar Province and, other major REE and HFSE-rich provinces around the world. We show that in most cases the primary δ^{34}S values of Gardar melts have not been significantly modified. Analysis of various Gardar magmatic suites reveals an overall ^{34}S-enriched but heterogeneous mantle source and commonality between trace element and S isotope systematics. In particular, the Late Gardar dykes of the Tuttutooq-Ilimmaasaq-Narsarsuaq zone, alkaline complexes, and clusters of silica-undersaturated dykes spatially associated with the alkaline complexes show marked enrichment in δ^{34}S, LILE, LREE and HFSE. We propose that subduction metasomatism associated with the Ketilidian orogeny (~500 Ma before rifting) created heterogeneous enrichment of the mantle lithosphere. This process is typified by enriched mantle domains and an overall northward decrease in the degree of metasomatism (consistent with the direction of subduction, Fig. 1b). Gardar alkaline complexes are spatially associated with mantle domains enriched in δ^{34}S, REE, HFSE and volatiles. We suggest this is no coincidence, and a lithospheric mantle source enriched in incompatible metals, alkalis and volatiles, which promote extreme differentiation of alkaline melts and fluids, is critical to the formation of alkaline ore deposits.

CRediT authorship contribution statement

William Hutchison: Conceptualization, Investigation, Methodology, Writing – original draft, Writing – review & editing. **Adrian A. Finch:** Conceptualization, Funding acquisition, Project administration, Resources, Writing – review & editing. **Anouk M. Borst:** Resources, Writing – review & editing. **Michael A.W. Marks:** Funding acquisition, Investigation, Resources, Writing – review & editing. **Brian G.J. Upton:** Resources, Writing – review & editing. **Aubrey L. Zerkle:** Methodology, Writing – review & editing. **Eva E. Stüeken:** Formal analysis, Methodology, Writing – review & editing. **Adrian J. Boyce:** Formal analysis, Methodology, Writing – review & editing.

Declaration of competing interest

The authors declare that they have no known competing financial interests or personal relationships that could have appeared to influence the work reported in this paper.

Acknowledgements

This work is a contribution to the HiTech AlkCarb project and was funded by the European Union's Horizon 2020 research and innovation programme under grant agreement No. 689909. W.H. also acknowledges support from a UKRI Future Leaders Fellowship (MR/S033505/1). A.J.B. is funded by the NERC National Environment Isotope Facility award (NE/S011587/1) and the Scottish Universities Environmental Research Centre. Technical assistance at SUERC was provided by A. MacDonald and at St Andrews by T. Di Rocco and C. Mettam. The manuscript greatly benefited from the two anonymous reviews and we would like to thank the reviewers for their pertinent and constructive comments, and Rosemary Hickey-Vargas for editorial handling.

Appendix A. Supplementary material

Supplementary material related to this article can be found online at https://doi.org/10.1016/j.epsl.2021.117034.

References

Aiuppa, A., Moretti, R., Federico, C., Giudice, G., Gurrieri, S., Liuzzo, M., Papale, P., Shinohara, H., Valenza, M., 2007. Forecasting Etna eruptions by real-time observation of volcanic gas composition. Geology 35, 1115–1118. https://doi.org/10.1130/G24149A.1.

Alt, J.C., Schwarzenbach, E.M., Früh-Green, G.L., Shanks, W.C., Bernasconi, S.M., Garrido, C.J., Crispini, L., Gaggero, L., Padrón-Navarta, J.A., Marchesi, C., 2013. The role of serpentinites in cycling of carbon and sulfur: seafloor serpentinization and subduction metamorphism. Lithos 178, 40–54. https://doi.org/10.1016/j.lithos.2012.12.006.

Anenburg, M., Mavrogenes, J.A., Frigo, C., Wall, F., 2020. Rare earth element mobility in and around carbonatites controlled by sodium, potassium, and silica. Sci. Adv. 6. https://doi.org/10.1126/sciadv.abb6570.

Arzamastsev, A.A., Vesolovskiy, R.V., Travin, A.V., Yudin, D.S., Belyatsky, B.V., 2017. Paleozoic tholeiitic magmatism of the Kola province: spatial distribution, age, and relation to alkaline magmatism. Petrology 25, 42–65. https://doi.org/10.1134/S0869591116060023.

Bartels, A., Nielsen, T.F., Lee, S.R., Upton, B.G.J., 2015. Petrological and geochemical characteristics of Mesoproterozoic dyke swarms in the Gardar Province, South Greenland: evidence for a major sub-continental lithospheric mantle component in the generation of the magmas. Mineral. Mag. 79, 909–939. https://doi.org/10.1180/minmag.2015.079.4.04.

Borst, A.M., Waight, T.E., Finch, A.A., Storey, M., Roux, P.J.L., 2019. Dating agpaitic rocks: a multi-system (U/Pb, Sm/Nd, Rb/Sr and $^{40}Ar/^{39}Ar$) isotopic study of layered nepheline syenites from the Ilímaussaq complex, Greenland. Lithos 324–325, 74–88. https://doi.org/10.1016/j.lithos.2018.10.037.

Canfield, D.E., Raiswell, R., Westrich, J.T., Reaves, C.M., Berner, R.A., 1986. The use of chromium reduction in the analysis of reduced inorganic sulfur in sediments and shales. Chem. Geol. 54, 149–155. https://doi.org/10.1016/0009-2541(86)90078-1.

Carr, M.J., Feigenson, M.D., Bennett, E.A., 1990. Incompatible element and isotopic evidence for tectonic control of source mixing and melt extraction along the Central American arc. Contrib. Mineral. Petrol. 105, 369–380. https://doi.org/10.1007/BF00286825.

Coulson, I.M., Goodenough, K.M., Pearce, N.J.G., Leng, M.J., 2003. Carbonatites and lamprophyres of the Gardar Province – a 'window' to the sub-Gardar mantle? Mineral. Mag. 67, 855–872. https://doi.org/10.1180/0026461036750148.

Downes, H., Balaganskaya, E., Beard, A., Liferovich, R., Demaiffe, D., 2005. Petrogenetic processes in the ultramafic, alkaline and carbonatitic magmatism in the Kola Alkaline Province: a review. Lithos 85, 48–75. https://doi.org/10.1016/j.lithos.2005.03.020.

Fiege, A., Holtz, F., Behrens, H., Mandeville, C.W., Shimizu, N., Crede, L.S., Göttlicher, J., 2015. Experimental investigation of the S and S-isotope distribution between H_2O–S±Cl fluids and basaltic melts during decompression. Chem. Geol. 393–394, 36–54. https://doi.org/10.1016/j.chemgeo.2014.11.012.

Finch, A.A., McCreath, J.A., Reekie, C.D.J., Hutchison, W., Ismaila, A., Armour-Brown, A., Andersen, T., Simonsen, S.L., 2019. From Mantle to Motzfeldt: a genetic model for syenite-hosted Ta,Nb-mineralisation. Ore Geol. Rev. 107, 402–416. https://doi.org/10.1016/j.oregeorev.2019.02.032.

Goodenough, K.M., Upton, B.G.J., Ellam, R.M., 2002. Long-term memory of subduction processes in the lithospheric mantle: Evidence from the geochemistry of basic dykes in the Gardar Province of South Greenland. J. Geol. Soc. Lond. 159, 705–714. https://doi.org/10.1144/0016-764901-154.

Grove, T.L., Till, C.B., Krawczynski, M.J., 2012. The role of H_2O in subduction zone magmatism. Annu. Rev. Earth Planet. Sci. 40, 413–439. https://doi.org/10.1146/annurev-earth-042711-105310.

Halama, R., Wenzel, T., Upton, B.G.J., Siebel, W., Markl, G., 2003. A geochemical and Sr-Nd-O isotopic study of the Proterozoic Eriksfjord Basalts, Gardar Province, South Greenland: reconstruction of an OIB signature in crustally contaminated rift-related basalts. Mineral. Mag. 67, 831–853. https://doi.org/10.1180/0026461036750147.

Hanley, J.J., Koga, K.T., 2018. Halogens in terrestrial and cosmic geochemical systems: abundances, geochemical behaviors, and analytical methods. In: Harlov, D.E., Aranovich, L. (Eds.), The Role of Halogens in Terrestrial and Extraterrestrial Geochemical Processes. Springer Geochemistry, p. 101.

Hulett, S.R.W., Simonetti, A., Rasbury, E.T., Hemming, N.G., 2016. Recycling of subducted crustal components into carbonatite melts revealed by boron isotopes. Nat. Geosci. 9, 904–908. https://doi.org/10.1038/ngeo2831.

Hutchison, W., Babiel, R.J., Finch, A.A., Marks, M.A.W., Markl, G., Boyce, A.J., Stüeken, E.E., Friis, H., Borst, A.M., Horsburgh, N.J., 2019. Sulphur isotopes of alkaline magmas unlock long-term records of crustal recycling on Earth. Nat. Commun. 10. https://doi.org/10.1038/s41467-019-12218-1.

Irvine, T.N., Baragar, W.R.A., 1971. A guide to the chemical classification of the common volcanic rocks. Can. J. Earth Sci. 8, 523–548. https://doi.org/10.1139/e71-055.

Jugo, P.J., Wilke, M., Botcharnikov, R.E., 2010. Sulfur K-edge XANES analysis of natural and synthetic basaltic glasses: Implications for S speciation and S content as function of oxygen fugacity. Geochim. Cosmochim. Acta 74, 5926–5938. https://doi.org/10.1016/j.gca.2010.07.022.

Kelemen, P.B., Hanghøj, K., Greene, A.R., 2003. One view of the geochemistry of subduction-related magmatic arcs, with an emphasis on primitive andesite and lower crust. In: Treatise on Geochemistry, 3–9, pp. 2–70.

Kogarko, L.N., 1990. Ore-forming potential of alkaline magmas. Lithos 26, 167–175. https://doi.org/10.1016/0024-4937(90)90046-4.

Kogarko, L.N., Lahaye, Y., Brey, G.P., 2010. Plume-related mantle source of super-large rare metal deposits from the Lovozero and Khibina massifs on the Kola Peninsula, Eastern part of Baltic Shield: Sr, Nd and Hf isotope systematics. Mineral. Petrol. 98, 197–208. https://doi.org/10.1007/s00710-009-0066-1.

Köhler, J., Schönenberger, J., Upton, B., Markl, G., 2009. Halogen and trace-element chemistry in the Gardar Province, South Greenland: subduction-related mantle metasomatism and fluid exsolution from alkalic melts. Lithos 113, 731–747. https://doi.org/10.1016/j.lithos.2009.07.004.

Krumrei, T.V., Pernicka, E., Kaliwoda, M., Markl, G., 2007. Volatiles in a peralkaline system: abiogenic hydrocarbons and F-Cl-Br systematics in the naujaite of the Ilímaussaq intrusion, South Greenland. Lithos 95, 298–314. https://doi.org/10.1016/j.lithos.2006.08.003.

Labidi, J., Cartigny, P., 2016. Negligible sulfur isotope fractionation during partial melting: Evidence from Garrett transform fault basalts, implications for the late-veneer and the Hadean matte. Earth Planet. Sci. Lett. 451, 196–207. https://doi.org/10.1016/j.epsl.2016.07.012.

Labidi, J., Cartigny, P., Jackson, M.G., 2015. Multiple sulfur isotope composition of oxidized Samoan melts and the implications of a sulfur isotope "mantle array" in chemical geodynamics. Earth Planet. Sci. Lett. 417, 28–39. https://doi.org/10.1016/j.epsl.2015.02.004.

Labidi, J., Cartigny, P., Moreira, M., 2013. Non-chondritic sulphur isotope composition of the terrestrial mantle. Nature 501, 208–211. https://doi.org/10.1038/nature12490.

Larsen, L.M., Steenfelt, A., 1974. Alkali loss and retention in an iron-rich peralkaline phonolite dyke from the Gardar province. Lithos 7, 81–90.

Lehmann, B., Nakai, S., Höhndorf, A., Brinckmann, J., Dulski, P., Hein, U.F., Masuda, A., 1994. REE mineralization at Gakara, Burundi: evidence for anomalous upper mantle in the western Rift Valley. Geochim. Cosmochim. Acta 58, 985–992.

Mandler, B.E., Grove, T.L., 2016. Controls on the stability and composition of amphibole in the Earth's mantle. Contrib. Mineral. Petrol. 171, 1–20. https://doi.org/10.1007/s00410-016-1281-5.

Marini, L., Moretti, R., Accornero, M., 2011. Sulfur isotopes in magmatic-hydrothermal systems, melts, and magmas. Rev. Mineral. Geochem. 73, 423–492. https://doi.org/10.2138/rmg.2011.73.14.

Marini, L., Paiotti, A., Principe, C., Ferrara, G., Cioni, R., 1994. Isotopic ratio and concentration of sulfur in the undersaturated alkaline magmas of Vulture Volcano (Italy). Bull. Volcanol. 56, 487–492. https://doi.org/10.1007/BF00302829.

Marks, M.A.W., Markl, G., 2015. The Ilímaussaq alkaline complex, South Greenland. In: Layered Intrusions. Springer, pp. 649–691.

Marks, M.A.W., Vennemann, T., Siebel, W., Markl, G., 2004. Nd-, O-, and H-isotopic evidence for complex, closed-system fluid evolution of the peralkaline Ilímaussaq intrusion, South Greenland. Geochim. Cosmochim. Acta 68, 3379–3395. https://doi.org/10.1016/j.gca.2003.12.008.

McCreath, J.A., Finch, A.A., Simonsen, S.L., Donaldson, C.H., Armour-Brown, A., 2012. Independent ages of magmatic and hydrothermal activity in alkaline igneous rocks: the Motzfeldt Centre, Gardar Province, South Greenland. Contrib. Mineral. Petrol. 163, 967–982. https://doi.org/10.1007/s00410-011-0709-1.

Ohmoto, H., Rye, R.O., 1979. Carbon and sulfur isotopes. In: Barnes, H.L. (Ed.), Geochemistry of Hydrothermal Ore Deposits. Wiley, New York, pp. 509–567.

Pilet, S., Baker, M.B., Stolper, E.M., 2008. Metasomatized lithosphere and the origin of alkaline lavas. Science 80 (320), 916–919. https://doi.org/10.1126/science.1156563.

Praharaj, T., Fortin, D., 2004. Determination of acid volatile sulfides and chromium reducible sulfides in Cu-Zn and Au mine tailings. Water Air Soil Pollut. 155, 35–50. https://doi.org/10.1023/B:WATE.0000026526.26339.c3.

Ribeiro, J.M., Stern, R.J., Kelley, K.A., Shaw, A.M., Martinez, F., Ohara, Y., 2015. Composition of the slab-derived fluids released beneath the Mariana forearc: Evidence for shallow dehydration of the subducting plate. Earth Planet. Sci. Lett. 418, 136–148. https://doi.org/10.1016/j.epsl.2015.02.018.

Rooney, T.O., Deering, C.D., 2014. Conditions of melt generation beneath the Taupo Volcanic Zone: the influence of heterogeneous mantle inputs on large-volume silicic systems. Geology 42, 3–6. https://doi.org/10.1130/G34868.1.

Scaillet, B., MacDonald, R., 2006. Experimental and thermodynamic constraints on the sulphur yield of peralkaline and metaluminous silicic flood eruptions. J. Petrol. 47, 1413–1437. https://doi.org/10.1093/petrology/egl016.

Schilling, J.G., Bergeron, M.B., Evans, R., 1980. Halogens in the mantle beneath the North Atlantic. Philos. Trans. R. Soc. Lond. Ser. A, Math. Phys. Sci. 297, 147–178. https://doi.org/10.1098/rsta.1980.0208.

Schönenberger, J., Markl, G., 2008. The magmatic and fluid evolution of the Motzfeldt intrusion in South Greenland: insights into the formation of agpaitic and miaskitic rocks. J. Petrol. 49, 1549–1577. https://doi.org/10.1093/petrology/egn037.

Smith, M.P., Moore, K., Kavecsánszki, D., Finch, A.A., Kynicky, J., Wall, F., 2016. From mantle to critical zone: a review of large and giant sized deposits of the rare earth elements. Geosci. Front. 7, 315–334. https://doi.org/10.1016/j.gsf.2015.12.006.

Sørensen, H., Andersen, T., Emeleus, C.H., Secher, K., Upton, B.G.J., Weidick, A., 2006. Geological Guide to South Greenland. Geological Survey of Denmark and Greenland, Copenhagen.

Sørrensen, H., 1992. Agpaitic nepheline syenites: a potential source of rare elements. Appl. Geochem. 7, 417–427. https://doi.org/10.1016/0883-2927(92)90003-L.

Stevenson, R., Upton, B.G.J., Steenfelt, A., 1997. Crust-mantle interaction in the evolution of the Ilimaussaq Complex, South Greenland: Nd isotopic studies. Lithos 40, 189–202.

Sun, S.-s., McDonough, W.F., 1989. Chemical and isotopic systematics of oceanic basalts: implications for mantle composition and processes. Geol. Soc. (Lond.) Spec. Publ. 42, 313–345. https://doi.org/10.1144/GSL.SP.1989.042.01.19.

Tsay, A., Zajacz, Z., Sanchez-Valle, C., 2014. Efficient mobilization and fractionation of rare-earth elements by aqueous fluids upon slab dehydration. Earth Planet. Sci. Lett. 398, 101–112. https://doi.org/10.1016/j.epsl.2014.04.042.

Upton, B.G.J., 1991. Gardar mantle xenoliths: Iglutalik, South Greenland. Groenlands Geol. Unders. Rapp. 150, 37–43.

Upton, B.G.J., 2013. Tectono-magmatic evolution of the younger Gardar southern rift, South Greenland. Geological Survey of Denmark and Greenland Bulletin.

Upton, B.G.J., Emeleus, C.H., Heaman, L.M., Goodenough, K.M., Finch, A.A., 2003. Magmatism of the mid-Proterozoic Gardar Province, South Greenland: chronology, petrogenesis and geological setting. Lithos 68, 43–65. https://doi.org/10.1016/S0024-4937(03)00030-6.

Upton, B.G.J., Stephenson, D., Martin, A.R., 1985. The Tugtutôq older giant dyke complex: mineralogy and geochemistry of an alkali gabbro-augite-syenite-foyaite association in the Gardar Province of South Greenland. Mineral. Mag. 49, 623–642. https://doi.org/10.1180/minmag.1985.049.354.01.

Upton, B.G.J., Thomas, J.E., 1980. The Tugtutoq Younger Giant Dyke Complex, South Greenland: fractional crystallization of transitional olivine basalt magma. J. Petrol. 21, 167–198.

Van Den Bleeken, G., Koga, K.T., 2015. Experimentally determined distribution of fluorine and chlorine upon hydrous slab melting, and implications for F–Cl cycling through subduction zones. Geochim. Cosmochim. Acta 171, 353–373.

van Keken, P.E., Hacker, B.R., Syracuse, E.M., Abers, G.A., 2011. Subduction factory: 4. Depth-dependent flux of H_2O from subducting slabs worldwide. J. Geophys. Res., Solid Earth 116. https://doi.org/10.1029/2010JB007922.

Wallace, P.J., Edmonds, M., 2011. The sulfur budget in magmas: evidence from melt inclusions, submarine glasses, and volcanic gas emissions. Rev. Mineral. Geochem. 73, 215–246.

Watt, S.F.L., Pyle, D.M., Mather, T.A., Naranjo, J.A., 2013. Arc magma compositions controlled by linked thermal and chemical gradients above the subducting slab. Geophys. Res. Lett. 40, 2550–2556. https://doi.org/10.1002/grl.50513.